









# Degradation, boosted with Fe<sup>2+</sup> ions, of ethylene glycol in oxygen-saturated aqueous solutions using the H<sub>2</sub>O<sub>2</sub>/UV-C oxidation system: a kinetic study

Timur Fazliev <sup>a</sup> , Mikhail Lyulyukin <sup>ab</sup> , Dmitry Yakhvarov <sup>b</sup> ,  
Oleg Sinyashin <sup>b</sup> , Vadim Yakovlev <sup>a</sup> , Denis Kozlov <sup>a</sup> ,  
Dmitry Selishchev <sup>a\*</sup> 

**a:** Boreskov Institute of Catalysis SB RAS , Novosibirsk 630090, Russia

**b:** Arbuzov Institute of Organic and Physical Chemistry KazSC RAS , Kazan 420088, Russia

\* Corresponding author: [selishchev@catalysis.ru](mailto:selishchev@catalysis.ru)



## Abstract

Ethylene glycol (EG) is commonly found as the main organic contaminant in airport runoff water during the cold season due to its use in the composition of de-icing fluids. Despite relatively low acute and chronic toxicity, EG may lead to a rapid growth of undesirable microbial biofilms in water bodies, thus reducing the concentration of dissolved oxygen and suppressing biodiversity. EG degradation using hydrogen peroxide activated with UV-C light (H<sub>2</sub>O<sub>2</sub>/UV-C) is a promising method of solving this problem because H<sub>2</sub>O<sub>2</sub> serves as a cheap and green oxidant and provides complete EG mineralization in aqueous solutions. This paper describes the results of the in-depth study on the effect of adding Fe<sup>2+</sup> ions and saturating the reaction solution with oxygen on EG degradation in the H<sub>2</sub>O<sub>2</sub>/UV system, showing the synergistic effect of both these factors on boosting the rate of EG removal and the depth of its mineralization. Comprehensive analysis of EG degradation and individual oxidation of key EG intermediates using TOC and HPLC methods revealed the roles of Fe<sup>2+</sup> ions and dissolved oxygen in the synergistic effect and allowed us to clarify the main pathways of EG degradation in this system.

## Key findings

- H<sub>2</sub>O<sub>2</sub>/UV C oxidation system provides complete mineralization of ethylene glycol (EG).
- Key intermediates of EG degradation are identified using HPLC analysis.
- Individual oxidation of EG intermediates reveals main pathways of EG degradation.
- Addition of Fe<sup>2+</sup> ions to H<sub>2</sub>O<sub>2</sub>/UV C system boosts EG mineralization rate.
- Saturation of reaction solution with air increases EG mineralization depth and rate.

© 2025, the Authors. This article is published in open access under the terms and conditions of the Creative Commons Attribution (CC BY) license (<http://creativecommons.org/licenses/by/4.0/>).

## 1. Introduction

The contribution of air transport to global logistics continues to grow after the COVID-19 pandemic. According to a joint ACI World-ICAO report [1], global passenger traffic reached 9.5 billion passengers in 2024, marking a full recovery to pre-pandemic (2019) levels. Modern airports are complex facilities with developed infrastructure, but they generate many emissions that include greenhouse gases (e.g., CO<sub>2</sub>), volatile organic compounds (VOCs), fuels, and lubricants [2–5]. Air pollution is a vital problem because airport operations substantially increase the pollution of

ground-level air in adjacent areas [6]. In addition, generated emissions affect water bodies near airports. Inorganic ions, ammonia, benzotriazoles, and polycyclic aromatic hydrocarbons are found as the main contaminants in airport runoff [4]. In north regions, glycol compounds, such as ethylene glycol (EG), diethylene glycol (DEG), and propylene glycol (PG), also play a crucial role for cold seasons because they are used as the key components of anti/de-icing fluids that depress freezing points to protect aircraft from snow and ice accumulation [5]. Four types of aircraft de-icing fluids (ADFs) with distinct compositions and specific properties serve different purposes [7]. Indeed, low-viscosity Type

## Accompanying information

### Article history

Received: 20.10.25

Revised: 27.11.25

Accepted: 02.12.25

Available online: 12.12.25

### Keywords

ethylene glycol (EG), wastewater treatment, advanced oxidation processes (AOPs), photodegradation, H<sub>2</sub>O<sub>2</sub>/UV-C, photo-Fenton

### Funding

This research was funded by the grant of the Ministry of Science and Higher Education of the Russian Federation for large scientific projects in priority areas of scientific and technological development (No. 075-15-2024-646).

### Supplementary information

Supplementary materials: [▶ READ](#)

Transparent peer review: [▶ READ](#)

### Sustainable Development Goals



I fluids provide de-icing effect and are used to remove ice deposits, while high-viscosity Type IV fluids provide long-term anti-icing effect due to the formation of protective coatings that prevent ice deposition during aircraft takeoff. A two-step treatment using ADFs of several types is a standard procedure in many airports nowadays [8]. Thus, anti/de-icing procedures may lead to environmental pollution with glycols and other components due to runoff of contaminated water and entrainment of ADFs from aircraft surface during the takeoff. The peak concentration of glycols in airport runoff predominantly depends on the weather conditions and can vary from 2 to 20,000 mg L<sup>-1</sup> due to the different levels of ADF consumption [5].

Application of specific glycol in ADFs commonly depends on its regional availability. According to the literature, PG-containing ADFs are commonly used in USA [9], while EG dominates in ADF compositions used in China, Russia, and Canada due to colder temperatures [10]. Ethylene glycol exhibits higher acute toxicity than propylene glycol as: the minimum lethal doses (MLDs) identified in rats are 3.8 g kg<sup>-1</sup> and 19.8 g kg<sup>-1</sup> for EG and PG, respectively [11]. In mammals, EG can be metabolized into glycolic and glyoxylic acids, whereas the accumulation of these acids leads to severe acidosis. Note that real acute toxicity of airport runoff water predominantly results from other additives used in ADFs, such as benzotriazoles [12–14]. Chronic toxicity of ethylene glycol is related to the formation of oxalic acid and precipitation of oxalates, leading to kidney damage [11]. These forms of chronic damage were found in fish after the long-term exposure to EG solutions, but they were observed at high EG concentrations ( $\geq 550$  mg L<sup>-1</sup> for fat-head minnows under exposure for 7 days) [15]. In addition to individual toxicity, the overall negative environmental impact of glycols results from a decrease in the concentration of dissolved oxygen (DO) due to growth of undesirable river biofilms (URBs) [16]. As noted by Exton et al. [17], this occurs after contamination events, especially during the spring season, when higher temperatures accelerate microbial growth. The phenomenon correlates with seasonal spikes in aqueous glycol concentrations from melting snow deposits near airports [18].

Several methods were proposed to reduce the impact of glycol emissions on the environment. Highly concentrated glycol solutions generated in de-icing areas can be collected using special mats, sewage systems, and vacuum trucks for further distillation and reuse [19]. However, this method is economically unviable for low-concentration glycol solutions (< 5%) due to high energy demands [20]. Controlled biodegradation in soil or wetlands [21,22] as well as an anaerobic oxidation [23] can be employed to treat low-concentrated glycol solutions. On the other hand, these biological systems are highly sensitive to glycol concentration, temperature ranges, and other contaminants. Given the seasonality and weather-dependent use of glycols, concentration spikes may overload biodegradation systems

[21,24]. Therefore, the development of efficient and low-cost method for treatment of airport runoff water is an urgent task.

The advanced oxidation processes (AOPs) are promising methods of solving the problem of water contamination with glycols. Hydrogen peroxide can be used as an effective, low-cost, and environmentally friendly oxidant for the degradation of organic contaminants. In contrast to KHSO<sub>5</sub> or K<sub>2</sub>S<sub>2</sub>O<sub>8</sub> oxidants, H<sub>2</sub>O<sub>2</sub> does not produce harmful by-products or inorganic salts, and its residuals can be easily removed using activated carbon or manganese oxide [25,26]. However, H<sub>2</sub>O<sub>2</sub> is to be properly activated to produce highly reactive  $\cdot$ OH radicals, which can efficiently oxidize organic pollutants due to their high redox potential (2.73 V vs. RHE) [27]. Different methods based on photochemical [28], sonochemical [29], photocatalytic [30], and electrochemical treatments [31], as well as Fenton and Fenton-like processes [32] were proposed and extensively studied. Photochemical activation of H<sub>2</sub>O<sub>2</sub> in aqueous solutions under their exposure to UV-C light is a powerful and easy-to-use technique that provides efficient degradation of organic pollutants. We have shown in our previous study [33] that EG is completely mineralized in the H<sub>2</sub>O<sub>2</sub>/UV-C oxidation system. Furthermore, the rate of EG mineralization in this system can be substantially boosted by purging the reaction solution with oxygen or air, especially at EG:H<sub>2</sub>O<sub>2</sub> ratios lower than the stoichiometric value.

Combination of different AOPs or several H<sub>2</sub>O<sub>2</sub> activation methods may result in the synergistic effect by increasing the efficiency of H<sub>2</sub>O<sub>2</sub> utilization. Thus, combination of ozonation and H<sub>2</sub>O<sub>2</sub>/UV-C treatment to remove micropollutants (pesticides and herbicides) led to the two-fold increase in the degradation efficiency [34]. Additional H<sub>2</sub>O<sub>2</sub> activation with UV-C light during the Fenton process (i.e. photo-Fenton) is regarded as a simple way to boost the oxidation process. Ghaly et al. [35] achieved the nine-fold increase in the rate constant of p-chlorophenol degradation after adding iron ions into the H<sub>2</sub>O<sub>2</sub>/UV oxidation system. McGinnis et al. [36] showed an increase in EG oxidation rate for the H<sub>2</sub>O<sub>2</sub>/UV-C system after pre-treatment with Fenton's reagent. However, there are few studies on EG mineralization using H<sub>2</sub>O<sub>2</sub> oxidant, and the mechanism of this process remains unclear. One of the main questions is the predominant pathway of EG degradation: a sequential route, as proposed by McGinnis et al. [36], or two parallel pathways terminating in formic acid and oxalic acid [33,37]. Furthermore, the origin of some by-products (e.g., formaldehyde) is either unclear or neglected. This work is aimed at in-depth study on the effect of Fe<sup>2+</sup> ions and oxygen on EG mineralization in the H<sub>2</sub>O<sub>2</sub>/UV oxidation system. The kinetic aspects of EG degradation and formation of oxidation intermediates are investigated under different reaction conditions, and the pathways of EG degradation are deeply discussed.

## 2. Materials and methods

### 2.1. Chemicals

Ethylene glycol (EG; AO Reachem Inc, Moscow, Russia) was used as a model glycol pollutant to perform the kinetic experiments on its mineralization. The purchased EG was diluted with deionized water to prepare a model EG solution with a concentration of 500 mg L<sup>-1</sup> (or 8 mM). The initial value of EG concentration was selected based on the results of a comprehensive review made by Sulej et al. [4]. The authors showed that EG concentration in airport drainage may vary in a wide range up to 20 g L<sup>-1</sup>. Furthermore, the concerned EG concentration is in consistent with the recent work published by Wang et al. [30], where chemical oxygen demand (COD) values of the samples from different airport locations including aircraft runways and rainwater collection tanks varied in the range of 400–600 mg L<sup>-1</sup>, thus corresponding to EG concentration of 300–465 mg L<sup>-1</sup>. Hydrogen peroxide (H<sub>2</sub>O<sub>2</sub>, 30%; Lega, Moscow, Russia) served as an oxidant. Prior to use, exact concentration of H<sub>2</sub>O<sub>2</sub> was measured via the titration using a standardized KMnO<sub>4</sub> solution. Ammonium iron(II) sulfate ((NH<sub>4</sub>)<sub>2</sub>Fe(SO<sub>4</sub>)<sub>2</sub>·6H<sub>2</sub>O, AO Reachem Inc), also known as Mohr's salt, was used as a source of Fe<sup>2+</sup> ions. Commercially available organic compounds, namely, glycolaldehyde (GD, Fluka Chemie GmbH, Buchs, Switzerland), glycolic acid (GA, BLD Pharmatech Ltd., Cincinnati, USA), glyoxylic acid (GxA, BLD Pharmatech Ltd.), oxalic acid (OA, BLD Pharmatech Ltd.), and formic acid (FA, AO Reachem Inc), were purchased to prepare model solutions for identification of EG oxidation intermediates using high-performance liquid chromatography (HPLC). Crystalline glyoxal (glyoxal trimer dihydrate, GL) was kindly provided by Novochem LLC (Tomsk, Russia).

### 2.2. Kinetic experiments

The kinetic experiments on EG mineralization were carried out in a 2.4 L cylindrical (30 cm in height and 10 cm in diameter) glass vessel externally covered with an aluminum jacket. A germicidal lamp (10 W, GPH212T5VH/4, Heraeus Group, Hanau, Germany) was used as a source of UV-C radiation. The lamp was housed into a quartz tube using a lab-made plastic holder. In routine experiments, the vessel was filled with 1 L of EG solution (500 mg L<sup>-1</sup>), and specific amounts of H<sub>2</sub>O<sub>2</sub> and Fe<sup>2+</sup> were added under continuous stirring. The quartz tube with lamp holder was then positioned in the center of vessel reactor. The reaction time started when the lamp was turned on. In a series of experiments with air bubbling, the reaction solution was additionally purged with air using PTFE tube immersed into the solution that provided air flow of 1 L min<sup>-1</sup> rate. The scheme of experimental setup and emission spectrum of UV-C lamp can be found in Figure S1 in the Supplementary materials. The matrix effect was investigated by addition of 2 M H<sub>2</sub>SO<sub>4</sub> or 1 M NaOH solutions to adjust pH prior to turning the UV lamp on. Addition of Na<sub>2</sub>SO<sub>4</sub> or NaBr to the concentration

of 10 mM was used to study the effects of ionic strength or quenching the formation of ·OH radicals, respectively [38].

### 2.3. Analysis of EG degradation

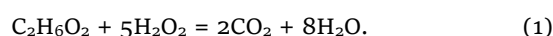
Liquid probes were sampled periodically from the reaction solution and analyzed using several methods to study the kinetics and EG degradation products. Total organic carbon (TOC) served as the main parameter of EG mineralization depth. TOC was measured using a TOC N/C multi 3100 total organic carbon analyzer (Analytik Jena GmbH, Jena, Germany). The concentrations of EG and major oxidation intermediates were analyzed by high-performance liquid chromatography (HPLC) using an Acquity Arc System (Waters Corporation, Milford, MA, USA) equipped with autosampler, quaternary solvent manager, 30 cm column manager with Repronmer H ion-exclusion column (Dr. Maisch HPLC GmbH, Ammerbuch, Germany), photodiode array detector (PDA), and refractive index detector (RID). HPLC analysis was performed within a minute interval after sampling to avoid interference with possible oxidation of intermediates by H<sub>2</sub>O<sub>2</sub> under the dark conditions. H<sub>2</sub>O<sub>2</sub> concentrations were analyzed by an enzymatic spectrophotometric method using commercial glucose oxidase reagent (Vector Best, Novosibirsk, Russia). Absorption spectra were recorded on a Cary 300 spectrophotometer (Agilent, Santa Clara, USA). Other details on TOC, H<sub>2</sub>O<sub>2</sub> and HPLC analyses can be found elsewhere [33]. The errors in these measurements did not exceed 5%.

The experiments on individual oxidation of key intermediates were additionally performed to discover the main reaction pathways of EG mineralization. In these experiments, each intermediate (i.e., GA, GxA, GD, GL, OA, FA) was used as a starting substrate instead of EG to carry out a routine kinetic experiment. Initial concentrations of H<sub>2</sub>O<sub>2</sub> and Fe<sup>2+</sup> were 40 mM and 5 mg L<sup>-1</sup>, respectively. Because the source of UV-C light was not changed in these experiments, the operational parameters were the same to achieve similar number of ·OH radicals generated from H<sub>2</sub>O<sub>2</sub>. The concentration of each intermediate was referenced to H<sub>2</sub>O<sub>2</sub> concentration to adjust stoichiometric ratio between intermediate and H<sub>2</sub>O<sub>2</sub> required for its complete mineralization.

## 3. Results and Discussion

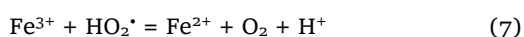
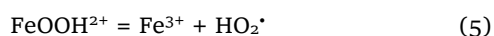
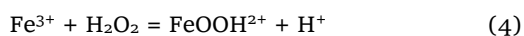
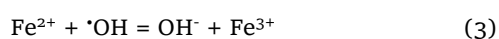
### 3.1. Effect of Fe<sup>2+</sup> concentration on the overall EG degradation rate

The effect of Fe<sup>2+</sup> ions on the degradation of ethylene glycol was evaluated in a batch photochemical reactor using H<sub>2</sub>O<sub>2</sub> as an oxidant under its activation with UV-C light (i.e., H<sub>2</sub>O<sub>2</sub>/Fe/UV-C system). The initial ratio between EG:H<sub>2</sub>O<sub>2</sub> components was adjusted to 1:5 to correspond to the stoichiometric ratio according to the following reaction of complete EG oxidation:

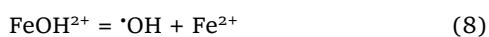


According to the UV-Vis optical absorption spectra (Figure S2), hydrogen peroxide can strongly absorb UV-C light and is the most photochemically active compounds in systems discussed. Activation of H<sub>2</sub>O<sub>2</sub> with UV-C light provides oxidative degradation of ethylene glycol due to the photo-generation of <sup>•</sup>OH radicals, which have high redox potential (2.73 V vs. RHE) and can efficiently oxidize organic compounds [27]. Complete oxidation of ethylene glycol (i.e., EG mineralization) is confirmed by decrease in TOC concentration under irradiation, as shown in Figure 1a (see TOC plot attributed to Fe<sup>2+</sup> concentration of 0 mg L<sup>-1</sup>).

Fenton and photo-Fenton AOPs are widely used in practice to decompose organic pollutants in water [39]. Fe<sup>2+</sup>/Fe<sup>3+</sup> redox pair plays a key role in these processes because easy transformations between iron charge states allows creating a catalytic system for generation of <sup>•</sup>OH radicals via the following equations [40,41]:



In the presence of Fe<sup>3+</sup> ions, generation of OH<sup>•</sup> radicals occurs under exposure to UV-C radiation:



Therefore, addition of Fe<sup>2+</sup> ions to the H<sub>2</sub>O<sub>2</sub>/UV-C system creates another pathway of H<sub>2</sub>O<sub>2</sub> activation and allows generation of more <sup>•</sup>OH radicals and other reactive species.

Ammonium iron(II) sulfate ((NH<sub>4</sub>)<sub>2</sub>Fe(SO<sub>4</sub>)<sub>2</sub>·6H<sub>2</sub>O) was added to the reaction solution as a source of Fe<sup>2+</sup> ions to create a photo-Fenton system. Initial Fe<sup>2+</sup> concentration was varied in the range from 0 to 7.5 mg L<sup>-1</sup>. TOC plots in Figure 1a show a substantial increase in the rate of EG mineralization after addition of Fe<sup>2+</sup> ions to the reaction solution. As follows from the plots, TOC removal rate increases as the Fe<sup>2+</sup> concentration increases because the reaction time required for 50% reduction in TOC is 140 min without addition of Fe<sup>2+</sup> ions and 48 min at a Fe<sup>2+</sup> concentration of 5 mg L<sup>-1</sup>. Note that Fe<sup>2+</sup> alone without exposure of the reaction solution to UV-C light has no effect on EG mineralization using H<sub>2</sub>O<sub>2</sub> because TOC change for 3 h under these conditions does not exceed an experimental error.

For clearer illustration of Fe<sup>2+</sup> effect, midrange regions of corresponding TOC plots (Figure 1a) were used to evaluate the EG mineralization rate (mg<sub>TOC</sub> L<sup>-1</sup> h<sup>-1</sup>). Figure 1c shows that the EG mineralization rate in the H<sub>2</sub>O<sub>2</sub>/Fe/UV-C system linearly depends on the initial concentration of Fe<sup>2+</sup> ions in the whole studied range up to 7.5 mg L<sup>-1</sup>. Similar

behavior was previously shown in several studies on degradation of different organic pollutants in a Fenton system [41–43]. For instance, Tokumura et al. [41] showed that concentration of <sup>•</sup>OH radicals linearly depends on Fe<sup>2+</sup> concentration in a photo-Fenton system at low Fe<sup>2+</sup> concentrations. This is caused by an increase in the number of H<sub>2</sub>O<sub>2</sub> activation sites in the reaction solution without significant undesirable scavenging or recombination of <sup>•</sup>OH radicals.

It is important to note that at the Fe<sup>2+</sup> concentration of 7.5 mg L<sup>-1</sup>, the final TOC level is higher than that observed in the other cases, thus indicating substantially lower mineralization depth at high Fe<sup>2+</sup> concentration. Figure S3 in the Supplementary materials shows that this behavior is reproduced in independent measurements. We suppose that it occurs due to fast decomposition of H<sub>2</sub>O<sub>2</sub> at a high Fe<sup>2+</sup> concentration without involving many generated <sup>•</sup>OH radicals into the target process and, consequently, their inefficient utilization. Based on the results of kinetic experiments, Fe<sup>2+</sup> concentration in the range of 5–7.5 mg L<sup>-1</sup> can be regarded as an optimum one for the H<sub>2</sub>O<sub>2</sub>/Fe/UV-C system because it provides both high rate and high depth of EG mineralization.

In our previous work [33], we have found that EG mineralization in the H<sub>2</sub>O<sub>2</sub>/UV-C system can be boosted by purging the reaction solution with oxygen or air: air purging with volume flow rate of 1 L min<sup>-1</sup> led to 43% increase in EG mineralization rate at initial EG:H<sub>2</sub>O<sub>2</sub> molar ratio of 1:5. Herein, we examine the effect of purging the reaction solution with air on EG mineralization in the presence of Fe<sup>2+</sup> ions (i.e., H<sub>2</sub>O<sub>2</sub>/Air/Fe/UV-C system).

Similarly to the previous case, midrange regions of corresponding TOC plots (Figure 1b) were used for the evaluation of EG mineralization rate (mg<sub>TOC</sub> L<sup>-1</sup> h<sup>-1</sup>) by their linear approximation. EG mineralization rate in the H<sub>2</sub>O<sub>2</sub>/Air/Fe/UV-C system also linearly depends on the initial concentration of added Fe<sup>2+</sup> ions in the range up to 5 mg L<sup>-1</sup> (Figure 1b). Comparing the rates in the H<sub>2</sub>O<sub>2</sub>/Fe/UV-C and H<sub>2</sub>O<sub>2</sub>/Air/Fe/UV-C systems allows us to conclude that the saturation of reaction mixture with oxygen via air purging increases both EG mineralization rate (in terms of absolute values) and rate enhancement effect due to addition of Fe<sup>2+</sup> ions (higher slope of approximation line for the H<sub>2</sub>O<sub>2</sub>/Air/Fe/UV-C system). Note that in contrast to the H<sub>2</sub>O<sub>2</sub>/Fe/UV-C system, the increase in Fe<sup>2+</sup> concentration from 5 to 7.5 mg L<sup>-1</sup> has lower effect in the H<sub>2</sub>O<sub>2</sub>/Air/Fe/UV-C system because EG mineralization rate does not increase proportionally (Figure 1c). It may occur due to the limitation of mineralization kinetics by photonic flux and radiation source being the same in all experiments described above because UV light is the key factor in this process. An increased Fe dosage may lead to excess generation of <sup>•</sup>OH radicals and, therefore, their recombination and scavenging [41]. Thus, Fe<sup>2+</sup> concentration of 5 mg L<sup>-1</sup> can be regarded as an optimum value in this system because it provides complete EG mineralization and leads to 4.4-fold increase in EG mineralization rate: from 59 mg L<sup>-1</sup> h<sup>-1</sup> for the case without addition of Fe<sup>2+</sup> to 262 mg L<sup>-1</sup> h<sup>-1</sup> for Fe<sup>2+</sup> concentration of 5 mg L<sup>-1</sup>.

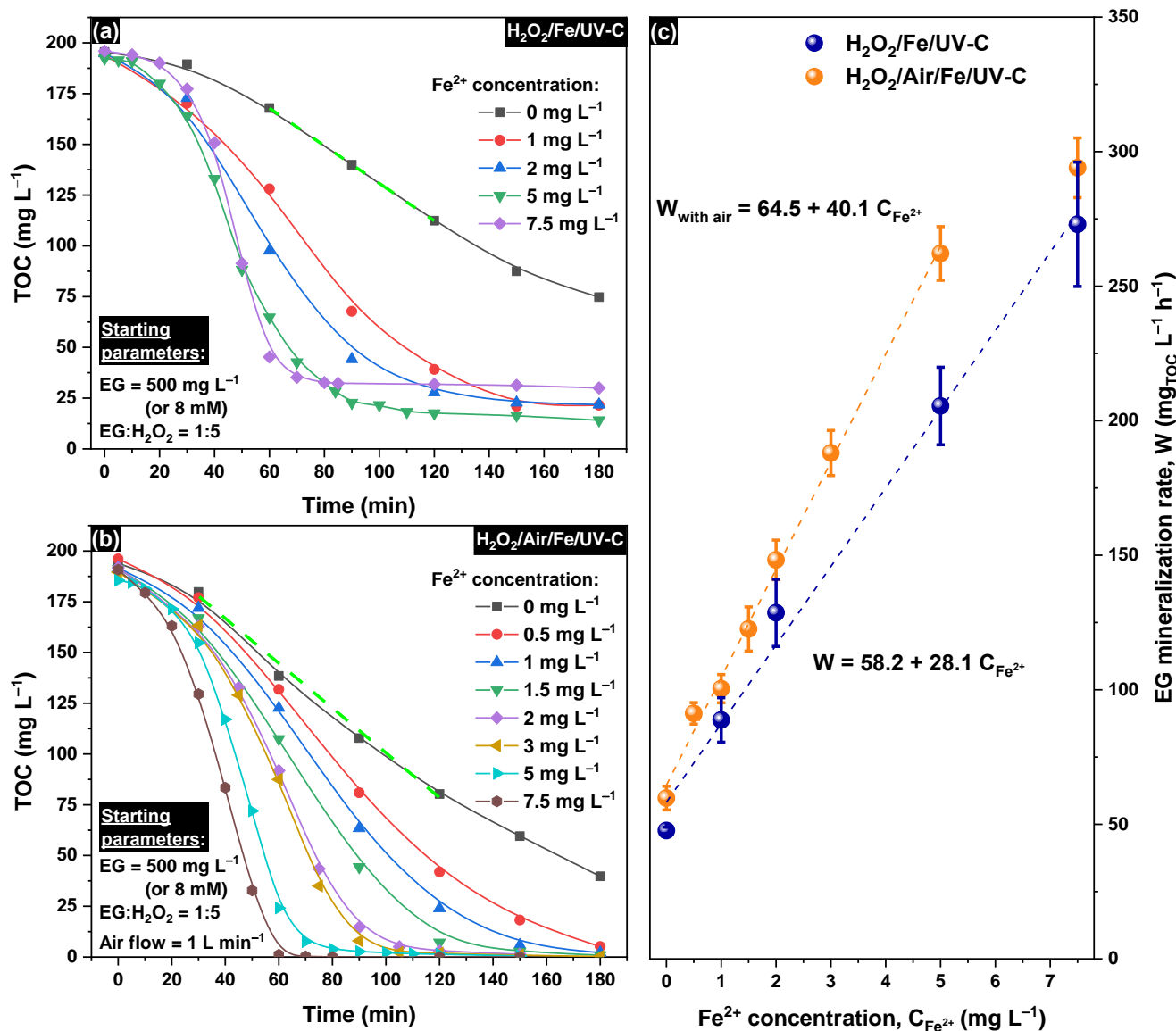


**Figure 1** TOC kinetic plots of EG mineralization in (a) H<sub>2</sub>O<sub>2</sub>/Fe/UV-C and (b) H<sub>2</sub>O<sub>2</sub>/Air/Fe/UV-C systems at different Fe<sup>2+</sup> concentrations ranged from 0 to 7.5 mg L<sup>-1</sup>; (c) effect of initial Fe<sup>2+</sup> concentration on EG mineralization rate in the H<sub>2</sub>O<sub>2</sub>/Fe/UV-C and H<sub>2</sub>O<sub>2</sub>/Air/Fe/UV-C systems.

As follows from the results discussed above, the addition of Fe<sup>2+</sup> ions with simultaneous saturation of the reaction solution with oxygen via air purging can be regarded as a cheap and easy-to-use approach to increase EG mineralization rate using H<sub>2</sub>O<sub>2</sub> activated with UV-C light. However, additional purification stage is needed because iron ion concentrations used are relatively high. Ion exchange [44], oxidation/filtration [45], physical absorbance (e.g., using activated carbon [46]), and other methods can be further employed to remove excessive iron species from water after the treatment process [47], thus preventing negative impact of these species on aquatic biota. Furthermore, ion exchange or oxidation/filtration allows iron to be simply recovered, regenerated, and reused in the process.

### 3.2. Kinetics of EG degradation in different oxidation systems

HPLC analysis allowed us to detect glycolaldehyde (GD), glycolic acid (GA), glyoxylic acid (GxA), glyoxal (GL),

formic acid (FA), oxalic acid (OA), and formaldehyde (FD) as the main intermediates of EG degradation in the H<sub>2</sub>O<sub>2</sub>/Fe/UV-C and H<sub>2</sub>O<sub>2</sub>/Air/Fe/UV-C systems. Similarly, to EG, these intermediates may have a hazardous effect on the environment; therefore, the treatment should provide complete mineralization of EG and all formed intermediates. The next step was the in-depth analysis of the kinetic aspects of EG removal and transformation of these intermediates under different conditions to establish reasons for the synergistic effect observed in the H<sub>2</sub>O<sub>2</sub>/Air/Fe/UV-C system under addition of Fe<sup>2+</sup> ions and saturation of the reaction solution with oxygen. The details on studied systems and their labels are listed in Table 1. The initial concentrations of EG and H<sub>2</sub>O<sub>2</sub> in all the experiments were 8 and 40 mM, respectively, thus corresponding to the stoichiometric ratio (Equation 1). The concentration of Fe<sup>2+</sup> ions was selected as 5 mg L<sup>-1</sup> based on the results discussed above.

**Table 1** Labels of EG oxidation systems with different combinations of reaction components.

Label of system	Addition of Fe <sup>2+</sup> ions <sup>a</sup>	Air purging <sup>b</sup>
H <sub>2</sub> O <sub>2</sub> /UV-C	-	-
H <sub>2</sub> O <sub>2</sub> /Air/UV-C	-	+
H <sub>2</sub> O <sub>2</sub> /Fe/UV-C	+	-
H <sub>2</sub> O <sub>2</sub> /Air/Fe/UV-C	+	+

<sup>a</sup> initial concentration of Fe<sup>2+</sup> ions corresponds to 5 mg L<sup>-1</sup>;

<sup>b</sup> air purging with a flow rate of 1 L min<sup>-1</sup>.

The concentration profiles of all detected reaction components are shown in Figure 2. These plots are divided into two groups combining initial pollutant (EG) and formed

intermediates (FA, OA, FD, GA, GD, GxA, GL) for clearer representation.

Figure 2a shows that complete removal of EG in the H<sub>2</sub>O<sub>2</sub>/UV-C system occurs for 75 min or less due to its oxidation to intermediate products. A sharp increase in the concentration of formaldehyde, formic acid, and glycolaldehyde occurs during the initial period of 0–20 min (Figure 2b) followed by a gradual decrease in their concentrations. Between 30 and 80 min, the concentrations of glyoxal and glycolic acid reach their maxima. This behavior can be attributed to a decrease in the oxidation rate of intermediates due to steadily declining H<sub>2</sub>O<sub>2</sub> concentration during the reaction.

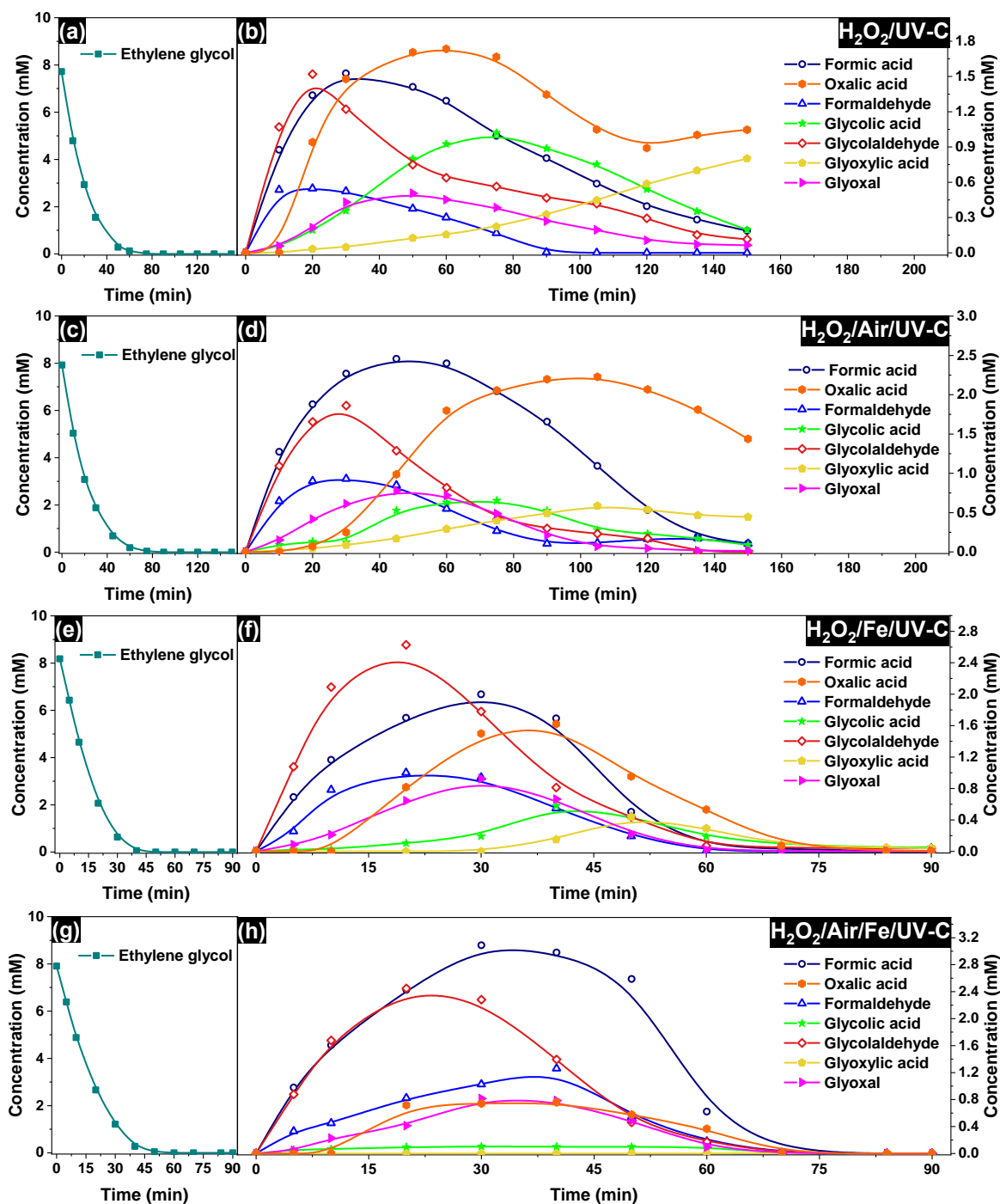


**Figure 2** Concentration profiles of EG and main oxidation intermediates during EG degradation under different conditions: (a, b) H<sub>2</sub>O<sub>2</sub>/UV-C; (c, d) H<sub>2</sub>O<sub>2</sub>/Air/UV-C; (e, f) H<sub>2</sub>O<sub>2</sub>/Fe/UV-C; (g, h) H<sub>2</sub>O<sub>2</sub>/Air/Fe/UV-C.

The main organic products are found in the solution after 150 min to be glyoxylic acid and oxalic acid. Accumulation of these acids probably occurs due to the depletion of  $\text{H}_2\text{O}_2$  because in the case of an insufficient amount of the oxidant, organic radicals generated under UV-C radiation can recombine with each other, thus decreasing the efficiency of mineralization. Note that in addition to main intermediates shown in Figure 2, traces of other intermediate compounds were observed during HPLC analysis. One of the peaks detected in chromatograms (Figure S4, Table S1) can be attributed to tartaric acid ( $\text{HOOC-CH}_2\text{OH-CH}_2\text{OH-COOH}$ ). According to the other published studies [48–51], formation of tartaric acid, tartronic acid, maleic acid, and oligomers of oxalic acid is possible due to the radical nature of mineralization process in the  $\text{H}_2\text{O}_2/\text{UV-C}$  system and recombination of  $\text{C}_2$  organic radicals.

Figure 2c,d shows that similar patterns are observed, when the reaction mixture is additionally purged with air (i.e.,  $\text{H}_2\text{O}_2/\text{Air}/\text{UV-C}$ ): complete removal of ethylene glycol occurs for 75 min; a rapid increase in the concentrations of formic acid, formaldehyde, and glycolaldehyde is observed during the first 20 min after the start of irradiation; an increase in the concentrations of intermediate oxidation products, such as glyoxal and glycolic acid, occurs in the period of 20–80 min; and glyoxylic acid and oxalic acid are found to be residual organic compounds in the solution after 150 min. The main differences are related to the concentrations of oxidation intermediates. Specifically, the concentrations of glycolic acid and glyoxylic acid under air purging are  $\sim 1.5$  times lower compared to those in the  $\text{H}_2\text{O}_2/\text{UV-C}$  system, whereas a two-fold increase in the maximum concentrations of formic acid and oxalic acid is observed. It can be assumed that saturation of the reaction solution with oxygen promotes oxidation of glycolic and glyoxylic acids to oxalic acid and its further mineralization, especially at low  $\text{H}_2\text{O}_2$  concentrations.

The kinetic plots for the  $\text{H}_2\text{O}_2/\text{Fe}/\text{UV-C}$  system (Figure 2e, f) clearly show the effect of  $\text{Fe}^{2+}$  ions on EG degradation using  $\text{H}_2\text{O}_2$  activated with UV-C light. Given the same order of intermediates as in the  $\text{H}_2\text{O}_2/\text{UV-C}$  system but specifically higher maximum concentration of glycolaldehyde,  $\text{Fe}^{2+}$  addition provides much higher rate of EG oxidation (Figure 2e) and increases the overall oxidation efficiency and mineralization of all intermediates (Figure 2f). Higher oxidation rate of formic and oxalic acids in the  $\text{H}_2\text{O}_2/\text{Fe}/\text{UV-C}$  system results in faster mineralization measured by TOC analysis, as they are the last step in the EG oxidation pathway before the complete mineralization to  $\text{CO}_2$ .

According to the kinetics of EG degradation in the  $\text{H}_2\text{O}_2/\text{Air}/\text{Fe}/\text{UV-C}$  system (Figure 2g, h), the positive effect of saturation with oxygen can be clearly seen in the plots of glyoxylic and glycolic acids because their detected concentrations are extremely low ( $<0.1$  mM) compared to the other cases. Despite the fact that the concentration profiles

of oxidation intermediates in the  $\text{H}_2\text{O}_2/\text{Air}/\text{Fe}/\text{UV-C}$  system are similar to those in the  $\text{H}_2\text{O}_2/\text{Air}/\text{UV-C}$  system, oxalic acid does not accumulate significantly because its concentration remains lower than 0.75 mM during the process. The concentration of formic acid also reduces much faster in the  $\text{H}_2\text{O}_2/\text{Air}/\text{Fe}/\text{UV-C}$  system (from 3.0 mM at 30 min to  $\sim 0$  at 70 min) than in the case of the  $\text{H}_2\text{O}_2/\text{Air}/\text{UV-C}$  system (from 2.5 mM at 45 min to  $\sim 0$  at 150 min). These observations support the conclusion that addition of  $\text{Fe}^{2+}$  ions increases the overall rate of EG mineralization.

To determine the direct effect of air or Fe on the activation of hydrogen peroxide,  $\text{H}_2\text{O}_2$  concentrations were measured during experiments in the described systems (Figure 3). Thus, it was found that additional air bubbling slightly reduces the rate of hydrogen peroxide consumption during the process. The presence of Fe ions, however, leads to a significantly faster decrease in  $\text{H}_2\text{O}_2$  concentration, which together with the higher rate of EG mineralization confirms an increase in efficiency and rate of hydrogen peroxide activation.

The concentrations of EG and intermediate oxidation products determined by HPLC allow calculation of both the TOC attributed to these compounds and the amount of hydrogen peroxide required for their complete mineralization. The calculated data are presented in Figure S5. The information obtained allows us to draw several important conclusions about the process.

First, in the case of the  $\text{H}_2\text{O}_2/\text{UV-C}$  system, a discrepancy is observed between calculated and experimentally obtained TOC data, which aligns with the hypothesis of organic radical recombination generating  $\text{C}_3\text{--C}_4$  compounds, particularly in the early stages of the process. However, these compounds remain unidentified. Since they are formed at the beginning of the process, their degree of mineralization relative to EG is low; therefore, they make a significant contribution to the discrepancy between the  $\text{H}_2\text{O}_2$  concentrations required for complete mineralization ( $\text{H}_2\text{O}_2_{\text{req}}$ ) and those determined experimentally ( $\text{H}_2\text{O}_2_{\text{exp}}$ ), reducing  $\text{H}_2\text{O}_2_{\text{req}}$ .

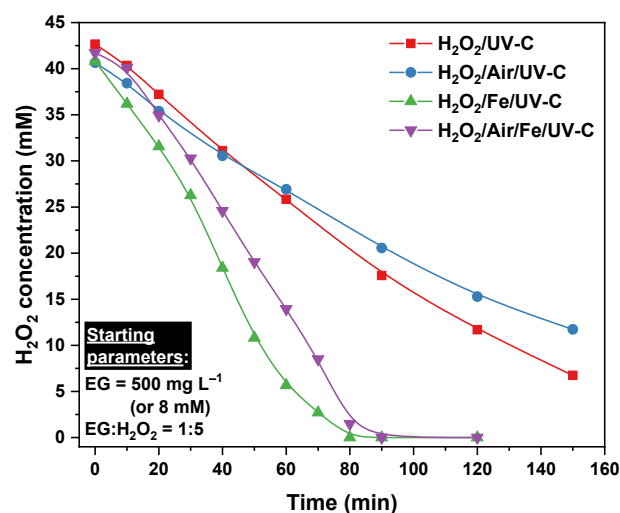
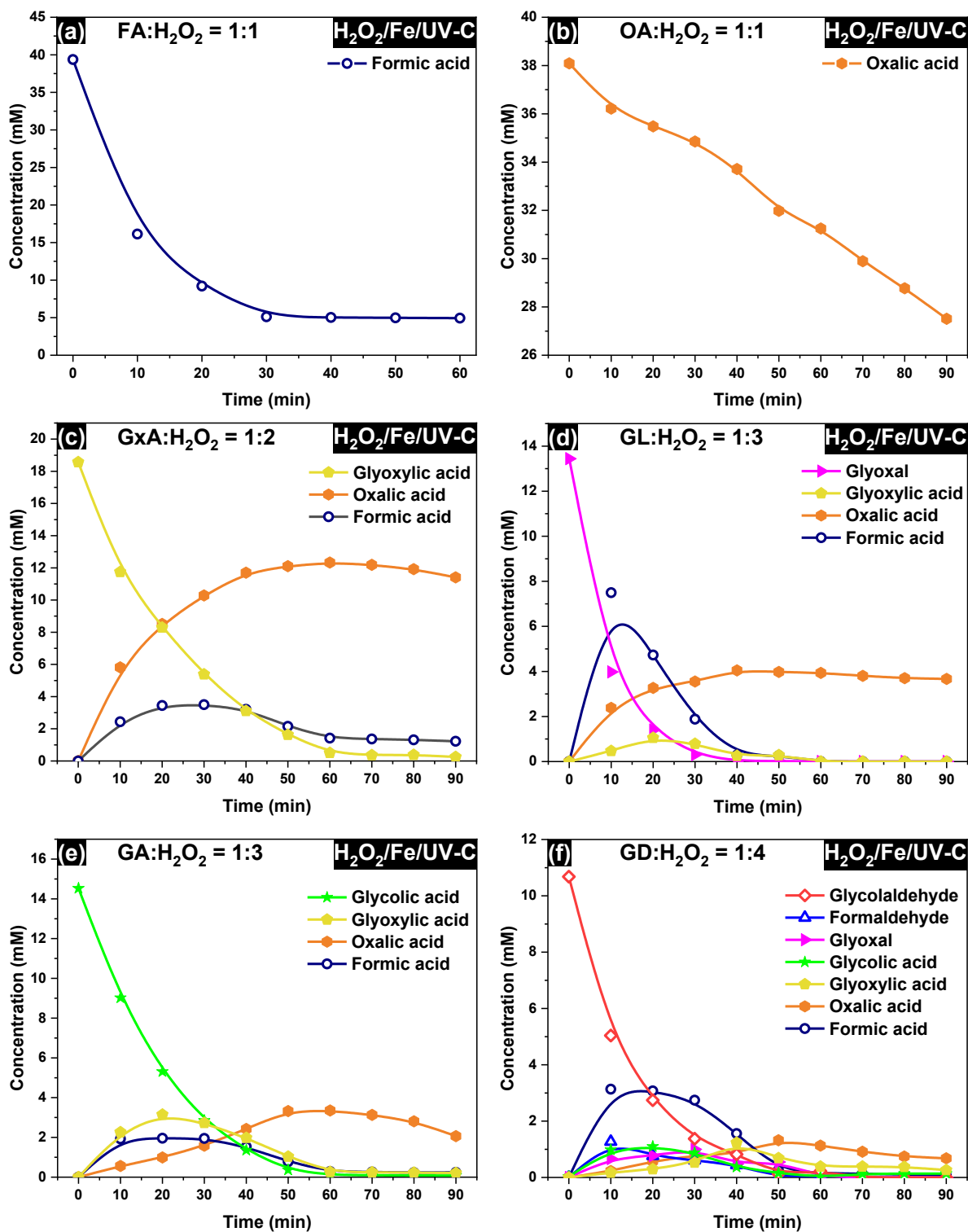


Figure 3  $\text{H}_2\text{O}_2$  concentration profiles during EG degradation under different conditions.

As the process proceeds, these organic compounds are also subjected to mineralization, and the discrepancy between the required and present amounts of  $H_2O_2$  decreases.

Second, considering the absence of significant differences between calculated and experimentally determined TOC, the reduction in the amount of hydrogen peroxide required relative to that present in solution upon aeration of the reaction mixture with air (in both  $H_2O_2$ /Air/UV-C and

$H_2O_2$ /Air/Fe/UV-C systems) confirms the role of  $O_2$  as an additional oxidizing agent. In the case of the  $H_2O_2$ /Fe/UV-C system, the difference between  $H_2O_2$  req and  $H_2O_2$  exp is insignificant. Nevertheless, the differences between calculated and experimentally determined TOC values may suggest the formation of unidentified organic compounds at the final stages of the process, when hydrogen peroxide concentration is low.



**Figure 4** Concentration profiles for individual degradation of major EG oxidation intermediates in the  $H_2O_2$ /Fe/UV-C system: (a) formic acid (FA: $H_2O_2$  = 1:1); (b) oxalic acid (OA: $H_2O_2$  = 1:1); (c) glyoxylic acid (GxA: $H_2O_2$  = 1:2); (d) glyoxal (GL: $H_2O_2$  = 1:3); (e) glycolic acid (GA: $H_2O_2$  = 1:3); (f) glycolaldehyde (GD: $H_2O_2$  = 1:4).

### 3.3. Pathways of EG degradation

Current knowledge regarding the pathways of EG oxidation in the  $\text{H}_2\text{O}_2/\text{UV-C}$  system remains limited. A series of additional experiments was performed to clarify the oxidation pathways and study the effect of  $\text{Fe}^{2+}$  ions and oxygen on the oxidation rate of intermediates. Formic acid (FA), oxalic acid (OA), glyoxylic acid (GxA), glycolic acid (GA), glyoxal (GL), and glycolaldehyde (GD) were oxidized individually in four different systems described in the previous section (see Table 1). The initial concentration of each intermediate compound was selected according to the stoichiometric ratio to  $\text{H}_2\text{O}_2$  concentration (40 mM) needed for its complete mineralization to  $\text{CO}_2$ .

Figure 4 shows as an example a set of the kinetic plots for the  $\text{H}_2\text{O}_2/\text{Fe}/\text{UV-C}$  system, whereas the results for other oxidation systems ( $\text{H}_2\text{O}_2/\text{UV-C}$ ,  $\text{H}_2\text{O}_2/\text{Air}/\text{UV-C}$ , and  $\text{H}_2\text{O}_2/\text{Air}/\text{Fe}/\text{UV-C}$ ) can be found in Figures S6–S8. Analysis of the kinetic aspects for key  $\text{C}_1$ – $\text{C}_2$  intermediates allows us to propose the main pathways of EG oxidation.

First, oxidation of formic acid (Figure 4a) and oxalic acid (Figure 4b) yields no detectable intermediates. This confirms that they are terminal products within their respective formation pathways. Conversely, significant FA concentration is observed during GxA oxidation (Figure 4c). While glyoxylic acid can be oxidized to formic acid by  $\text{H}_2\text{O}_2$  even under dark conditions [51] (Figure S6), this reaction pathway has not been previously discussed in the context of EG oxidation using the  $\text{H}_2\text{O}_2/\text{UV-C}$  systems [36,37,52,53]. A decrease in FA concentration after 30 min of reaction with simultaneous continuous growth in OA concentration supports our previous assumption that consecutive oxidation of  $\text{C}_2$  compounds plays an important role at the late stage of degradation, while C–C cleavage occurs predominantly during the first several minutes [33].

The intermediates detected during glyoxal oxidation are formic acid, glyoxylic acid, and oxalic acid (Figure 4d). Although glyoxal can be easily oxidized to formic acid by an excess of  $\text{H}_2\text{O}_2$  with formation of two FA molecules [54], oxalic acid becomes the dominant organic compound in our

system after extended reaction time. Oxidation of glycolic acid results in the formation of GxA, FA, and OA (Figure 4e). Similarity in FA and GxA concentration profiles, coupled with lower FA concentration compared to the cases of GL or GxA oxidation, allows us to propose no direct oxidation of glycolic acid to formic acid. Finally, the oxidation of glycolaldehyde yields formaldehyde, glyoxal, formic acid, oxalic acid, and glycolic acid (Figure 4f). It seems that among all studied compounds, GD is the only one that can yield detectable amounts of formaldehyde as the product of photolysis or oxidation [55].

As shown in Figures S6–S8, similar behavior (i.e., the same order of oxidation products and similar kinetics) is observed for individual oxidation of EG intermediates in all studied oxidation systems. These findings enable us to propose the main pathways of EG oxidation that occur in the  $\text{H}_2\text{O}_2/\text{UV-C}$  system (Figure 5). First, ethylene glycol oxidizes to glycolaldehyde, which can further form formaldehyde, glyoxal, and glycolic acid. Glyoxal and glycolic acid can be oxidized to glyoxylic acid, whereas glyoxylic acid can form formic and oxalic acids. Oxidation of oxalic and formic acids is the last step that limits complete EG mineralization to  $\text{CO}_2$ . After starting the irradiation, oxidation process predominantly occurs via C–C cleavage step due to the presence of higher amounts of  $\text{H}_2\text{O}_2$  and, consequently, higher number of photogenerated  $\cdot\text{OH}$  radicals. At the late stages, consecutive oxidation of  $\text{C}_2$  intermediates begins to prevail. These data completely confirm and expand our previous results [33]. To the best of our knowledge, this proposed scheme of EG degradation in the  $\text{H}_2\text{O}_2/\text{UV-C}$  system considers the formation of formaldehyde as one of the main oxidation intermediates for the first time and clearly demonstrates the presence of two parallel pathways with formic and oxalic acids as the last steps during EG degradation, prior to  $\text{CO}_2$  formation.

Concentration profiles of intermediates during their individual degradation in different oxidation systems are shown in Figure 5. Initial reaction rates were employed to illustrate the effect of  $\text{Fe}^{2+}$  ions and oxygen on the oxidation rate of intermediates (Table 2).

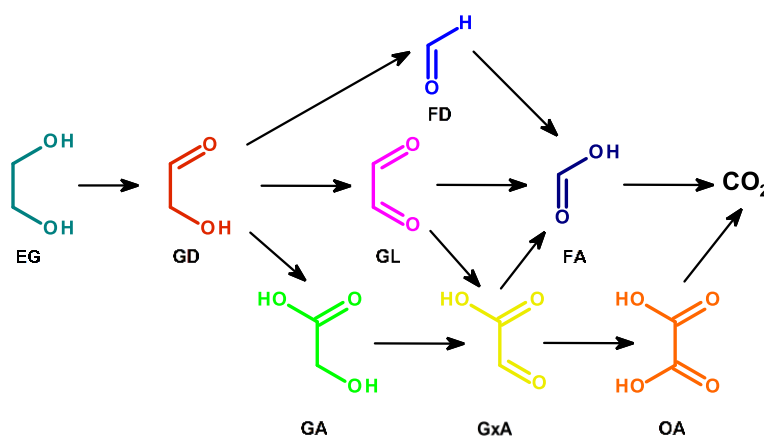


**Figure 5** Proposed scheme of EG degradation using  $\text{H}_2\text{O}_2$  activated with UV-C light.

According to the kinetic data shown in Table 2, oxalic acid (Figure 6b) seems to be more difficult-to-oxidize substance than formic acid (Figure 6a), probably due to its higher light absorbance in the UV-C region and consequent reduction in the number of  $\cdot\text{OH}$  radicals formed from  $\text{H}_2\text{O}_2$

under its activation with UV-C light. Therefore, it may limit EG mineralization rate at the late stages of oxidation process. GxA (Figure 6c), GA (Figure 6e), GD (Figure 6f) exhibit similar oxidation rate, whereas glyoxal is oxidized slightly faster than the other substances (Figure 5d).

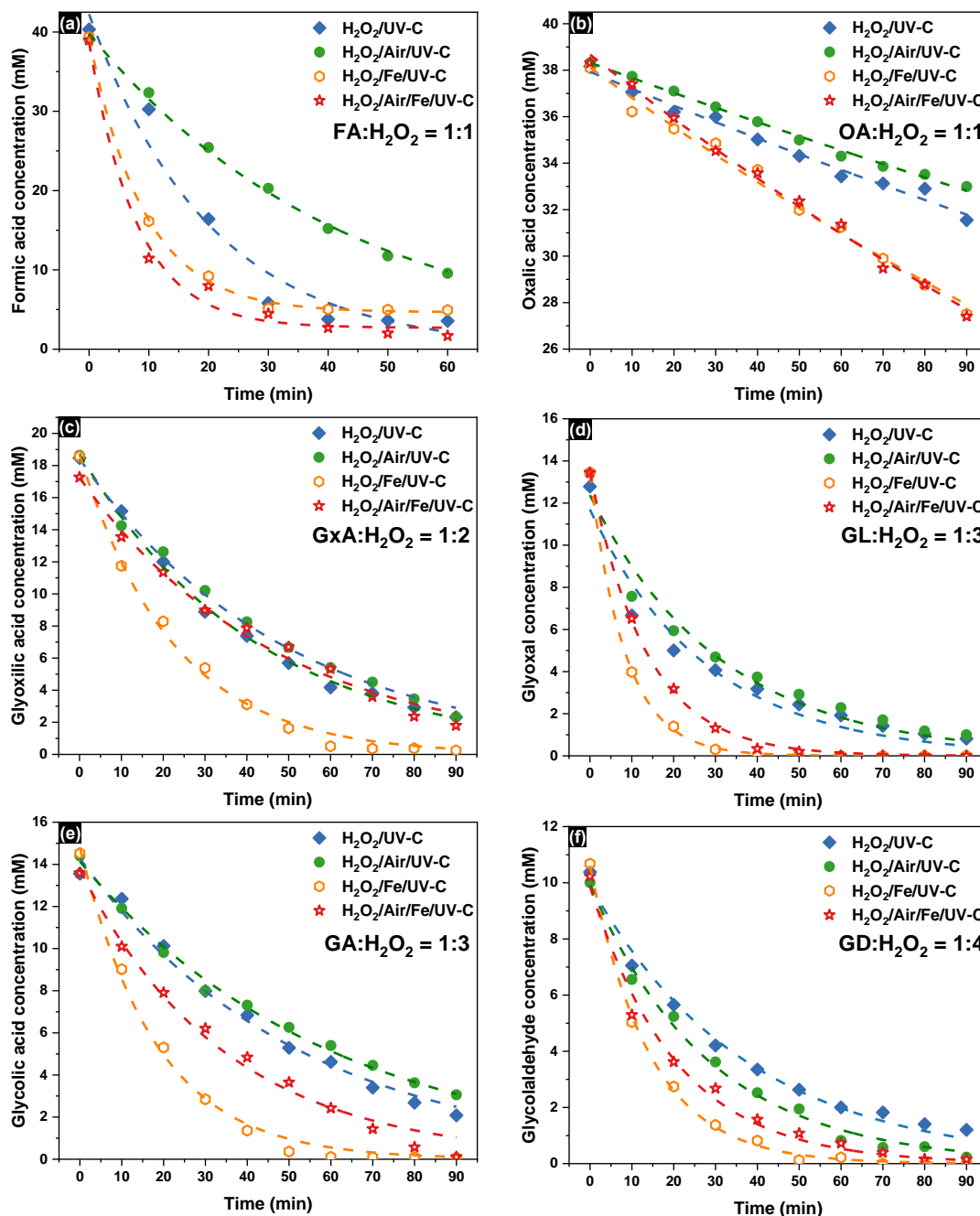


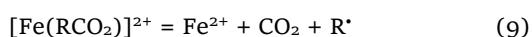
**Figure 6** Kinetic plots of EG intermediates oxidation in different systems: (a) formic acid ( $\text{FA}:\text{H}_2\text{O}_2 = 1:1$ ); (b) oxalic acid ( $\text{OA}:\text{H}_2\text{O}_2 = 1:1$ ); (c) glyoxylic acid ( $\text{GxA}:\text{H}_2\text{O}_2 = 1:2$ ); (d) glyoxal ( $\text{GL}:\text{H}_2\text{O}_2 = 1:3$ ); (e) glycolic acid ( $\text{GA}:\text{H}_2\text{O}_2 = 1:3$ ); (f) glycolaldehyde ( $\text{GD}:\text{H}_2\text{O}_2 = 1:4$ ).

**Table 2** Initial reaction rates for individual oxidation of EG intermediates.

EG oxidation intermediate	Initial rate ( $\text{mM min}^{-1}$ )			
	$\text{H}_2\text{O}_2/\text{UV-C}$	$\text{H}_2\text{O}_2/\text{Air}/\text{UV-C}$	$\text{H}_2\text{O}_2/\text{Fe}/\text{UV-C}$	$\text{H}_2\text{O}_2/\text{Air}/\text{Fe}/\text{UV-C}$
Formic acid	$1.17 \pm 0.05$	$0.63 \pm 0.3$	$2.32^a$	$2.75^a$
Oxalic acid	$0.068 \pm 0.003$	$0.061 \pm 0.001$	$0.114 \pm 0.003$	$0.122 \pm 0.002$
Glyoxylic acid	$0.319 \pm 0.003$	$0.24 \pm 0.03$	$0.43 \pm 0.07$	$0.27 \pm 0.02$
Glycolic acid	$0.18 \pm 0.01$	$0.19 \pm 0.02$	$0.39 \pm 0.05$	$0.21 \pm 0.02$
Glyoxal	$0.28 \pm 0.09$	$0.28 \pm 0.07$	$0.6 \pm 0.2$	$0.5 \pm 0.1$
Glycolaldehyde	$0.20 \pm 0.03$	$0.20 \pm 0.03$	$0.4 \pm 0.1$	$0.33 \pm 0.1$

<sup>a</sup>These initial rates were estimated using only two points due to the lack of experimental data and are given without error.

Table 2 shows that addition of  $\text{Fe}^{2+}$  ions ( $5 \text{ mg L}^{-1}$ ,  $\text{H}_2\text{O}_2/\text{Fe}/\text{UV-C}$  system) leads to two-fold or greater increase in the oxidation rate of all the EG intermediates compared with the  $\text{H}_2\text{O}_2/\text{UV-C}$  system. In addition to activation of  $\text{H}_2\text{O}_2$  via interaction with iron species as shown in Equations 2–8, complexation of iron with organic compounds can be considered to describe this behavior. Fe species can directly act as an oxidation factor via forming complexes with intermediate products and their further oxidation [56,57]. For instance,  $\text{Fe}^{3+}$  complexes with organic acids ( $[\text{Fe}(\text{RCO}_2)]^{2+}$ ) can be decarboxylized under exposure to UV light, thus reducing required amount of  $\text{H}_2\text{O}_2$  and increasing the efficiency of its utilization as well as regenerating  $\text{Fe}^{2+}$  ions as follows [43]:



Furthermore, special attention is to be paid to the *in situ* formation of the ferrioxalate system ( $[\text{Fe}(\text{C}_2\text{O}_4)_3]^{3+}$ ) during the EG oxidation in the presence of iron ions, which can also participate in the generation of reactive species under UV-C radiation and promote  $\text{Fe}^{3+}$  photoreduction [58].

Quite surprisingly, saturation of the reaction solution with oxygen both in the  $\text{H}_2\text{O}_2/\text{Air}/\text{UV-C}$  and  $\text{H}_2\text{O}_2/\text{Air}/\text{Fe}/\text{UV-C}$  systems predominantly leads to decrease in the oxidation rate in the case of formic acid and to a slight decrease in the oxidation rate for the other compounds. As shown by Aristova et al. [59], excess of oxygen results in the formation of  $\text{HO}_2^{\cdot}$  radicals via the following reaction:



These radicals cannot take part in oxidation processes, thus reducing mineralization rate of formic acid. However, there is a contradiction with the kinetics of EG mineralization (Figure 1), when the addition of oxygen increases the mineralization rate and its depth. At the same time, oxygen may act as an oxidant, especially at low  $\text{H}_2\text{O}_2$  concentrations, recombining with UV-generated organic radicals and mineralizing residual organic compounds [60]. For instance,

kinetic plots shown in Figure 6a indicate that simultaneous air purging and  $\text{Fe}^{2+}$  adding ( $\text{H}_2\text{O}_2/\text{Air}/\text{Fe}/\text{UV-C}$  system) result in fast mineralization of formic acid and increase its mineralization depth in comparison with the  $\text{H}_2\text{O}_2/\text{Fe}/\text{UV-C}$  system. Another illustrative example that supports this assumption is the kinetics of glyoxal oxidation in the  $\text{H}_2\text{O}_2/\text{Fe}/\text{UV-C}$  and  $\text{H}_2\text{O}_2/\text{Air}/\text{Fe}/\text{UV-C}$  systems (Figure 7). Without air purging, the concentration of oxalic acid reaches steady-state level (4 mM) after 40 min, whereas it continues to decrease under further irradiation in the case of  $\text{H}_2\text{O}_2/\text{Air}/\text{Fe}/\text{UV-C}$  system.

The results of this study allow the conclusion that the synergistic effect between addition of  $\text{Fe}^{2+}$  ions and saturation of the reaction solution with oxygen consists in participation of iron ions as a guiding factor in the oxidation of intermediates by additional  $\text{H}_2\text{O}_2$  activation and complexation of organic molecules, whereas oxygen serves as an oxidant at the late stages of this process.

### 3.4. pH and matrix effects on EG degradation

The other operating parameters, namely, pH and the presence of additional ions in the reaction solution that can suppress the formation of reactive species (i.e., matrix effect), may affect the efficiency of water treatment, because the studied process of EG degradation is radical-based and utilizes iron ions for boosted  $\text{H}_2\text{O}_2$  activation.

First, a change in pH of the reaction solution was studied under irradiation in the  $\text{H}_2\text{O}_2/\text{Fe}/\text{UV-C}$  and  $\text{H}_2\text{O}_2/\text{Air}/\text{Fe}/\text{UV-C}$  systems. In aqueous solutions containing  $\text{H}_2\text{O}_2$  and EG, starting pH values are commonly in the range of 6.2–6.5, whereas the addition of Mohr's salt to Fe concentration of  $5 \text{ mg L}^{-1}$  decreases pH to 4.7–4.8 (Figure 8). This fact is caused by the oxidation of  $\text{Fe}^{2+}$  by hydrogen peroxide to  $\text{Fe}^{3+}$  and subsequent hydrolysis of these ions. When the UV lamp is turned on, a gradual decrease in pH occurs in both systems down to a level of  $\sim 3.9$ , followed by a reversion to 4.5 in the case of  $\text{H}_2\text{O}_2/\text{Fe}/\text{UV-C}$  system (Figure 8a) or to 4.7, which is the same as the starting pH value, in the  $\text{H}_2\text{O}_2/\text{Air}/\text{Fe}/\text{UV-C}$  system (Figure 8b), respectively.

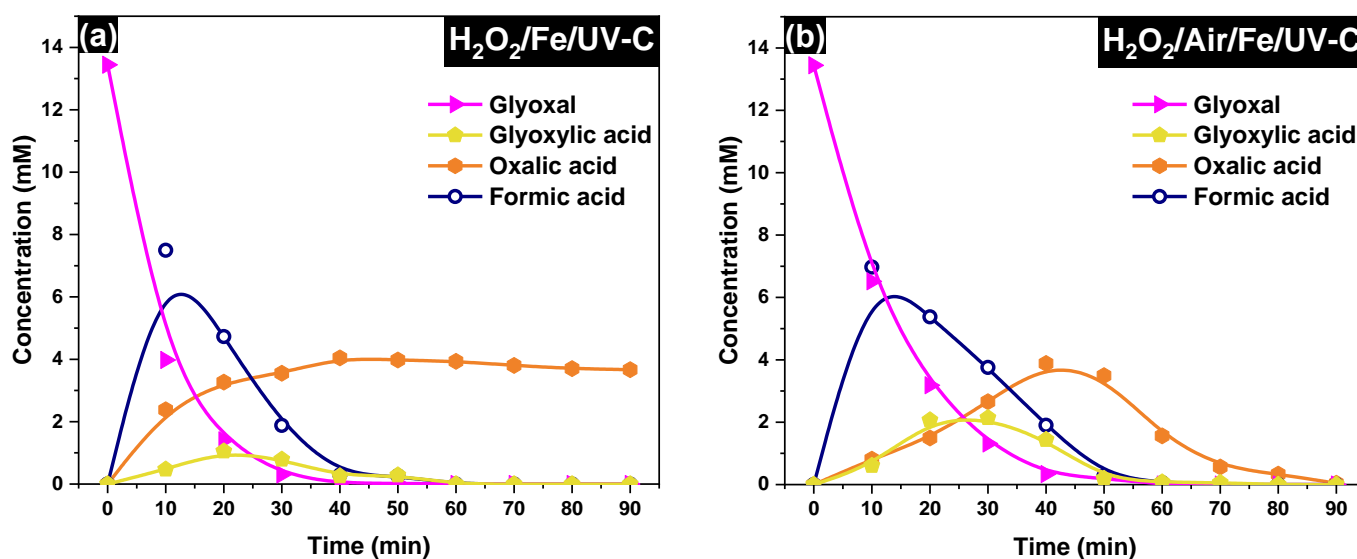


Figure 7 Concentration profiles of GL and its oxidation intermediates in (a)  $\text{H}_2\text{O}_2/\text{Fe}/\text{UV-C}$  and (b)  $\text{H}_2\text{O}_2/\text{Air}/\text{Fe}/\text{UV-C}$  systems ( $\text{GL}:\text{H}_2\text{O}_2 = 1:3$ ).

Figure 8 also shows the total concentration profiles of organic acid intermediates, and it is clear for both systems that pH changes in the opposite way to a change in the concentration of organic acids: pH decreases as the concentration of these acids increases and vice versa. Thus, comparison of the kinetic plots allows the conclusion that a change in pH of the reaction solution under irradiation in the studied systems occurs due to the formation of organic acid intermediates, predominantly formic and oxalic acids.

Note that slight inconsistency in the final pH values after the treatment in both systems (Figure 8) can be related to different values of residual  $\text{CO}_2$  content. Indeed, air flow in the  $\text{H}_2\text{O}_2/\text{Air}/\text{Fe}/\text{UV-C}$  system can promote the removal of  $\text{CO}_2$  from the solution, thus reducing its effect on pH.

It is well known that pH has a strong effect on the efficiency of Fenton and photo-Fenton processes [61–63]. We studied the dependence of EG mineralization rate on the initial pH value in the  $\text{H}_2\text{O}_2/\text{Air}/\text{Fe}/\text{UV-C}$  system, which provided the highest efficiency of EG degradation. The initial pH was adjusted by adding sulfuric acid or sodium hydroxide to the reaction solution containing  $\text{H}_2\text{O}_2$ , EG, and Mohr's salt prior to turning the UV lamp on.

TOC kinetic plots in Figure 9a show that initial pH has a strong effect on EG mineralization in the  $\text{H}_2\text{O}_2/\text{Air}/\text{Fe}/\text{UV-C}$  system. Both strongly acidic (pH 2.5) and alkali (pH 11.5–13.5) conditions provides low efficiency of EG degradation. Similarly to Figure 1, midrange regions of corresponding TOC plots were used to evaluate EG mineralization rate ( $\text{mg}_{\text{TOC}} \text{L}^{-1} \text{h}^{-1}$ ). Figure 9b shows that the mineralization rate has a dome-shaped dependence on initial pH, when the highest rate is achieved at pH 4.8. These conditions correspond to the initial system without adding pH modifiers.

While a decrease in EG mineralization rate at higher pH values can be accounted for by a decrease in iron solubility, a decrease in the mineralization rate at lower pH values has more complicated nature. As previously shown by Duesterberg et al. [64], the oxidation of formic acid by a Fenton reagent has the highest rate at pH 4.0 within the studied range from 2.5 to 4.0. The authors related this behavior to a decrease in Fe(II) regeneration rate at lower pH. Furthermore, superoxide radical ( $\text{O}_2^{\cdot-}$ ) can be easier protonated under acidic conditions to  $\text{HO}_2^{\cdot}$  radical, which is less reactive than  $\cdot\text{OH}$  radical. Concentration of  $\text{Fe}(\text{OH})_2^{2+}$  ion, which plays an important role in photo-Fenton process (Equation 8), also decreases at lower pH [65].

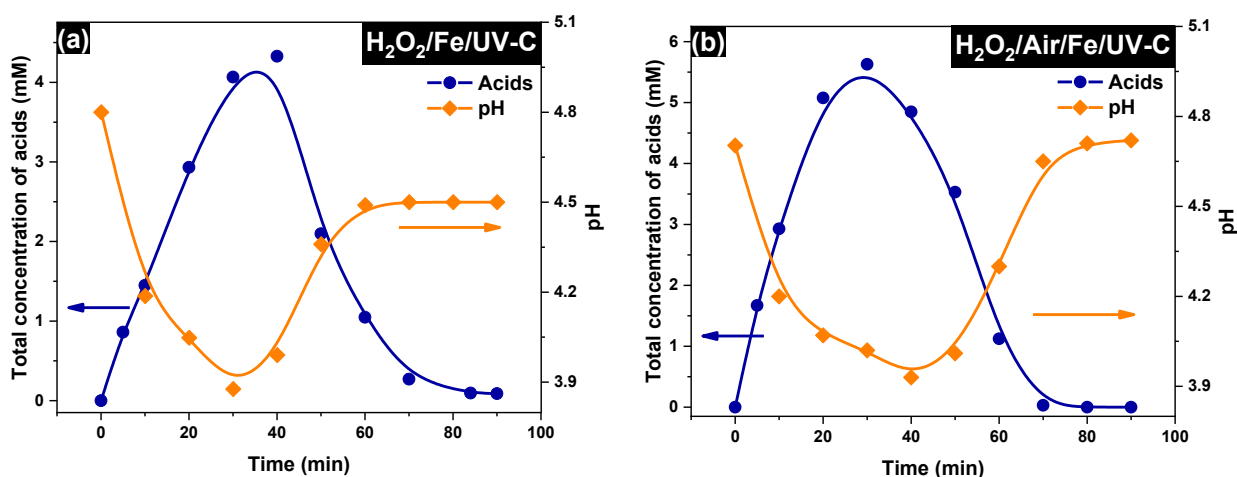


Figure 8 Time profiles of total concentration of acids and pH in (a)  $\text{H}_2\text{O}_2/\text{Fe}/\text{UV-C}$  and (b)  $\text{H}_2\text{O}_2/\text{Air}/\text{Fe}/\text{UV-C}$  systems.

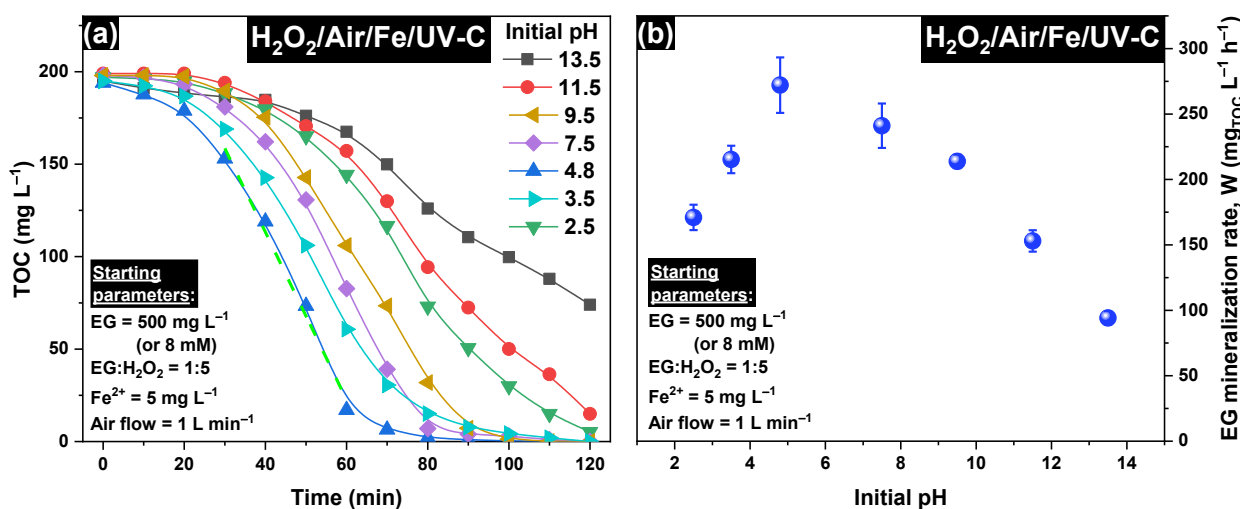
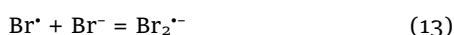


Figure 9 (a) TOC kinetic plots of EG mineralization in the  $\text{H}_2\text{O}_2/\text{Air}/\text{Fe}/\text{UV-C}$  system at different initial pH values; (b) effect of initial pH on EG mineralization rate in the  $\text{H}_2\text{O}_2/\text{Air}/\text{Fe}/\text{UV-C}$  system.

To isolate the effect of salinity from that of pH, we performed a specific experiment, in which an aliquot of 10 mM Na<sub>2</sub>SO<sub>4</sub> solution was added to the initial system. Figure 10 shows that salinity by itself has no significant effect on EG degradation process in the H<sub>2</sub>O<sub>2</sub>/Air/Fe/UV-C system, because TOC kinetic plot of EG mineralization after addition of Na<sub>2</sub>SO<sub>4</sub> is similar to that observed for the initial system. Complete mineralization of ethylene glycol occurs for 80 min in both these cases.

Similar experiment with adding an aliquot of 10 mM NaBr solution was made to confirm the predominant role of <sup>•</sup>OH radicals in the studied oxidation process. Bromide ions can react with <sup>•</sup>OH radicals as follows [38]:



Therefore, the addition of bromide ions to the reaction solution can substantially reduce the number of photogenerated <sup>•</sup>OH radicals and suppress the overall rate of oxidation process, because the formed Br<sub>2</sub><sup>•-</sup> radicals have lower oxidation potential (1.62 V vs. RHE) than <sup>•</sup>OH radicals [66]. Indeed, Figure 10 shows that the presence of <sup>•</sup>OH quenching agent completely suppresses EG mineralization, because TOC slightly reduces from 195 to 185 mg L<sup>-1</sup> for 120 min of irradiation. This result proves the predominant role of <sup>•</sup>OH radicals among all possible ROS in the proposed H<sub>2</sub>O<sub>2</sub>/Air/Fe/UV-C system.

Despite the fact that the use of this oxidative system is envisioned in either flow or batch mode with subsequent treatment of the processed wastewater to remove the added iron ions and discharge of the purified water, a cyclic experiment with the H<sub>2</sub>O<sub>2</sub>/Air/Fe/UV-C system was performed to verify the stability of this system, with intermediate addition of new portions of EG and H<sub>2</sub>O<sub>2</sub>. It was found that during this experiment there is no significant change in the rate of EG mineralization, which indicates the stability of the system (Figure 11).

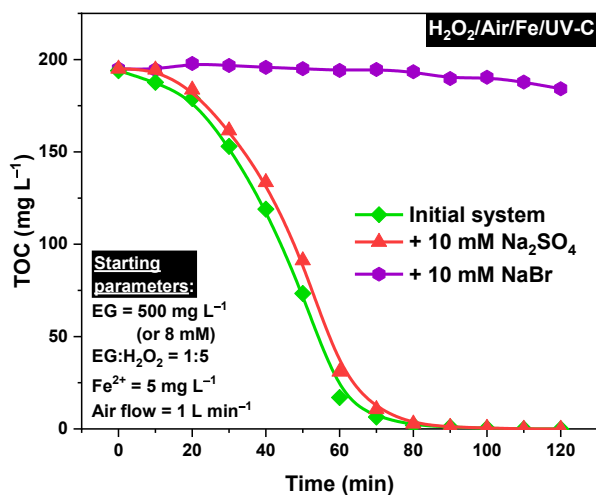


**Figure 10** Effect of matrix modification on TOC kinetic plots of EG mineralization in the H<sub>2</sub>O<sub>2</sub>/Air/Fe/UV-C system.

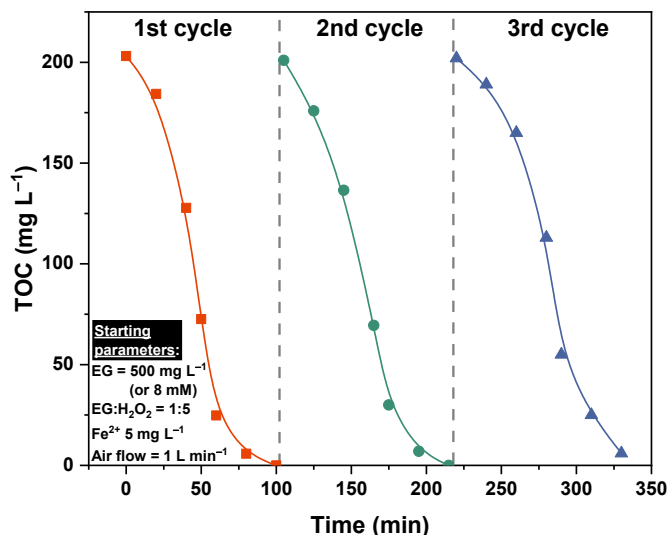


**Figure 11** TOC kinetic plots of EG mineralization in the H<sub>2</sub>O<sub>2</sub>/Air/Fe/UV-C system in cyclic experiments.

The results discussed above reveal a need for investigation and optimization of the specific parameters, such as ionic composition and pH of aqueous solution, prior to implementation of water treatment to achieve the highest efficiency of purification process.

## 4. Limitations

It should be noted that this study was not aimed at selecting the most optimal parameters of the process under investigation to reduce operational costs, nor did it address the impact of additional agents (ions, corrosion inhibitors, etc.), which are undoubtedly present in airport stormwater and may negatively affect the process. This study was primarily focused on investigating the kinetic features of the phenomenon discovered and the pathways of ethylene glycol mineralization as the key contaminant. The complexity and multi-parameter nature of real airport wastewater systems requires a significantly broader investigation to evaluate the effects of all potential wastewater components on EG mineralization rate, which is beyond the scope of the current work. Therefore, the methodology developed herein represents a foundational approach for effective EG mineralization that was examined independently of the broader compositional and operational aspects of real wastewater treatment systems. Future work is expected to involve research using real EG-containing airport wastewater, as well as the scaling up and optimization of the methodology described in this paper.

## 5. Conclusions

Activation of H<sub>2</sub>O<sub>2</sub> with UV-C light (H<sub>2</sub>O<sub>2</sub>/UV-C system) provides complete mineralization of ethylene glycol (EG) in aqueous solutions. The addition of Fe<sup>2+</sup> ions to the reaction solution (H<sub>2</sub>O<sub>2</sub>/Fe/UV-C system) boosts EG degradation, and its mineralization rate in this system linearly depends on the initial concentration of Fe<sup>2+</sup> ions in the whole studied

range up to 7.5 mg L<sup>-1</sup>. Thus, TOC removal rate increases by 6 times from 47 mg L<sup>-1</sup> h<sup>-1</sup> for the Fe-free system to 273 mg L<sup>-1</sup> h<sup>-1</sup> for the H<sub>2</sub>O<sub>2</sub>/Fe/UV-C system at Fe<sup>2+</sup> concentration of 7.5 mg L<sup>-1</sup> and super stoichiometric ratio of H<sub>2</sub>O<sub>2</sub> to EG (i.e., EG:H<sub>2</sub>O<sub>2</sub> = 1:5). Further enhancement can be achieved by additional oxygen saturation via purging the reaction solution with air flow of 1 L min<sup>-1</sup> (H<sub>2</sub>O<sub>2</sub>/Air/Fe/UV-C system) that increases both rate and depth of mineralization, thus enabling complete TOC removal for 60 min under optimum conditions. Comprehensive analysis of EG degradation and individual oxidation of key EG intermediates under different conditions reveals the roles of Fe<sup>2+</sup> ions and dissolved oxygen in the synergistic effect and allows discovering the main pathways of EG degradation. Iron ions substantially improve the oxidation efficiency by directing reaction pathways via additional H<sub>2</sub>O<sub>2</sub> activation and complexation of organic intermediates. While dissolved oxygen initially reduces oxidation rate, it becomes crucial for achievement of complete mineralization serving as additional oxidant with respect to H<sub>2</sub>O<sub>2</sub> at the late stages of the process. At the same time, •OH radicals have the predominant role in the proposed H<sub>2</sub>O<sub>2</sub>/Air/Fe/UV-C system. The results of this study highlight the importance of multiple interacting factors in advanced oxidation processes (AOPs) to decrease negative environmental impact of contaminants and improve the efficiency of water purification with reduced resource consumption.

### Supplementary materials

The supplementary materials are available on the corresponding online page. **Figure S1:** (a) Photo and schematic diagram of the photoreactor used for the kinetic experiments; (b) emission spectrum of UV-C germicidal lamp. **Figure S2:** Absorption spectra of water solutions containing EG, Fe<sup>2+</sup>, H<sub>2</sub>O<sub>2</sub>, and the reaction mixture after the experiment in H<sub>2</sub>O<sub>2</sub>/Fe/UV-C system.

**Figure S3:** Reproducibility of TOC plots for two independent experiments in the H<sub>2</sub>O<sub>2</sub>/Fe/UV-C system with [Fe<sup>2+</sup>]<sub>0</sub> = 7.5 mg L<sup>-1</sup>.

**Figure S4:** Examples of HPLC chromatograms of the reaction medium during the oxidation of glyoxal (H<sub>2</sub>O<sub>2</sub>/Air/UV-C, irradiation for 20 min).

**Figure S5:** Experimental and calculated TOC and H<sub>2</sub>O<sub>2</sub> concentration profiles in different oxidation systems: (a) H<sub>2</sub>O<sub>2</sub>/UV-C; (b) H<sub>2</sub>O<sub>2</sub>/Air/UV-C; (c) H<sub>2</sub>O<sub>2</sub>/Fe/UV-C; (d) H<sub>2</sub>O<sub>2</sub>/Air/Fe/UV-C.

**Figure S6:** Concentration profiles of GxA, OA, and FA in GxA oxidation by H<sub>2</sub>O<sub>2</sub> under dark conditions.

**Figure S7:** Concentration profiles for individual degradation of major EG oxidation intermediates in the H<sub>2</sub>O<sub>2</sub>/UV-C system: (a) formic acid (FA:H<sub>2</sub>O<sub>2</sub> = 1:1); (b) oxalic acid (OA:H<sub>2</sub>O<sub>2</sub> = 1:1); (c) glyoxylic acid (GxA:H<sub>2</sub>O<sub>2</sub> = 1:2); (d) glyoxal (GL:H<sub>2</sub>O<sub>2</sub> = 1:3); (e) glycolic acid (GA:H<sub>2</sub>O<sub>2</sub> = 1:3); (f) glycolaldehyde (GD:H<sub>2</sub>O<sub>2</sub> = 1:4).

**Figure S8:** Concentration profiles for individual degradation of major EG oxidation intermediates in the H<sub>2</sub>O<sub>2</sub>/Air/UV-C system: (a) formic acid (FA:H<sub>2</sub>O<sub>2</sub> = 1:1); (b) oxalic acid (OA:H<sub>2</sub>O<sub>2</sub> = 1:1); (c) glyoxylic acid (GxA:H<sub>2</sub>O<sub>2</sub> = 1:2); (d) glyoxal (GL:H<sub>2</sub>O<sub>2</sub> = 1:3); (e) glycolic acid (GA:H<sub>2</sub>O<sub>2</sub> = 1:3); (f) glycolaldehyde (GD:H<sub>2</sub>O<sub>2</sub> = 1:4).

**Figure S9:** Concentration profiles for individual degradation of major EG oxidation intermediates in the H<sub>2</sub>O<sub>2</sub>/Air/Fe/UV-C system: (a) formic acid (FA:H<sub>2</sub>O<sub>2</sub> = 1:1); (b) oxalic acid (OA:H<sub>2</sub>O<sub>2</sub> = 1:1); (c) glyoxylic acid (GxA:H<sub>2</sub>O<sub>2</sub> = 1:2); (d) glyoxal (GL:H<sub>2</sub>O<sub>2</sub> = 1:3); (e) glycolic acid (GA:H<sub>2</sub>O<sub>2</sub> = 1:3); (f) glycolaldehyde (GD:H<sub>2</sub>O<sub>2</sub> = 1:4).

**Table S1:** Retention times of organic compounds detected in the reaction medium via HPLC.

### Data availability statement

The data are available on request from the authors.

### Acknowledgment

None.

### Author contributions

Conceptualization: O.S., V.Y., D.K., D.S.

Data curation: T.F., M.L.

Formal Analysis: T.F., D.S.

Funding acquisition: O.S.,

Investigation: T.F., M.L.,

Methodology: M.L., D.K., D.S.

Project administration: D.Y., V.Y.,

Resources: D.Y., V.Y., D.K.,

Validation: M.L., D.Y., O.S., D.K., D.S.

Visualization: T.F., M.L., D.S.

Writing – original draft: T.F.

Writing – review & editing: D.S.

### Conflict of interest

The authors declare no conflict of interest.

### Additional information

Author IDs:

Timur Fazliev, Scopus ID [59515740100](https://orcid.org/0000-0001-5951-5740);

Mikhail Lyulyukin, Scopus ID [36988668600](https://orcid.org/0000-0001-3698-8668);

Dmitry Yakhvarov, Scopus ID [6602121810](https://orcid.org/0000-0001-6602-1218);

Oleg Sinyashin, Scopus ID [57188848065](https://orcid.org/0000-0001-5718-8848);

Vadim Yakovlev, Scopus ID [7201907594](https://orcid.org/0000-0001-7201-9075);

Denis Kozlov, Scopus ID [35366492500](https://orcid.org/0000-0001-3536-6492);

Dmitry Selishchev, Scopus ID [35436247300](https://orcid.org/0000-0001-3543-6247).

Websites:

Boreskov Institute of Catalysis, <https://en.catalysis.ru/>;

Arbuzov Institute of Organic and Physical Chemistry, <https://en.iopc.ru/>.

### References

1. Joint ACI World-ICAO Passenger Traffic Report, Trends, and Outlook. ACI World [Internet] 2025[cited 2025]. English. Available from: <https://aci.aero/2025/01/28/joint-aci-world-icao-passenger-traffic-report-trends-and-outlook/>, Accessed on 17 June 2025.
2. Lai C-H, Chuang K-Y, Chang J-W. Source Apportionment of Volatile Organic Compounds at an International Airport. *Aerosol Air Qual Res.* 2013;13:689–698. doi:[10.4209/aaqr.2012.05.0121](https://doi.org/10.4209/aaqr.2012.05.0121)
3. Nunes LM, Zhu Y-G, Stigter TY, Monteiro JP, Teixeira, MR. Environmental Impacts on Soil and Groundwater at Airports: Origin, Contaminants of Concern and Environmental Risks. *J Environ Monit.* 2011;13:3026–3039. doi:[10.1039/C1EM10458F](https://doi.org/10.1039/C1EM10458F)
4. Sulej AM, Polkowska Ż, Namieśnik J. Analysis of Airport Runoff Waters. *Critical Reviews in Analytical Chemistry* 2011;41:190–213. doi:[10.1080/10408347.2011.588920](https://doi.org/10.1080/10408347.2011.588920)
5. Sulej-Suchomska AM, Szumińska D, de la Guardia M, Przybyłowski P, Polkowska Ż. Airport Runoff Water: State-of-the-Art and Future Perspectives. *Sustainability.* 2024;16:8176. doi:[10.3390/su16188176](https://doi.org/10.3390/su16188176)
6. Masiol M, Harrison RM. Aircraft Engine Exhaust Emissions and Other Airport-Related Contributions to Ambient Air Pollution: A Review. *Atmospheric Environment.* 2014;95:409–55. doi:[10.1016/j.atmosenv.2014.05.070](https://doi.org/10.1016/j.atmosenv.2014.05.070)
7. Dyer KP. Anti-icing fluid residues. *SAE Trans.* [Internet] 2007[cited 2025];116:618–625. English. Available from <https://www.jstor.org/stable/44719495>, Accessed on 29 July 2025.

8. Gray DR. Environmental impact of aircraft deicing. Designing, Constructing, Maintaining, and Financing Today's Airport Projects. 2012;1–10. doi:[10.1061/40646\(2003\)25](https://doi.org/10.1061/40646(2003)25)
9. LaFond-Hudson S, Corsi SR, Rutter TD. Apportionment of oxygen demand contributions from aircraft and pavement deicer freezing point depressants in airport runoff, Milwaukee, Wisconsin, 2005–2022. *Integr Environ Assess Manag.* 2025;21:594–603. doi:[10.1093/inteam/vjae047](https://doi.org/10.1093/inteam/vjae047)
10. Zhang W, Zhang J, Chen S. Frost resistance of roller compacted concrete in airport runway subjected to ethylene glycol solution. *Anti-Corros Method Mater.* 2018;66:40–44. doi:[10.1108/ACMM-03-2018-1916](https://doi.org/10.1108/ACMM-03-2018-1916)
11. LaKind JS, McKenna EA, Hubner RP, Tardiff RG. A review of the comparative mammalian toxicity of ethylene glycol and propylene glycol. *Crit Rev Toxicol.* 1999;29:331–65. doi:[10.1080/10408449991349230](https://doi.org/10.1080/10408449991349230)
12. Cornell JS, Pillard DA, Hernandez MT. Comparative measures of the toxicity of component chemicals in aircraft deicing fluid. *Environ Toxicol Chem.* 2000;19:1465–72. doi:[10.1002/etc.5620190601](https://doi.org/10.1002/etc.5620190601)
13. Gruden CL, Hernandez M. Anaerobic digestion of aircraft deicing fluid wastes: Interactions and toxicity of corrosion inhibitors and surfactants. *Water Environ Res.* 2002;74:149–58. doi:[10.2175/106143002X139866](https://doi.org/10.2175/106143002X139866)
14. Pillard DA, Cornell JS, DuFresne, DL, Hernandez MT. Toxicity of benzotriazole and benzotriazole derivatives to three aquatic species. *Water Res.* 2001;35:557–60. doi:[10.1016/S0043-1354\(00\)00268-2](https://doi.org/10.1016/S0043-1354(00)00268-2)
15. Hartwell SI, Jordahl DM, Evans JE, May EB. Toxicity of aircraft de-icer and anti-icer solutions to aquatic organisms. *Environ Toxicol Chem.* 1995;14:1375–86. doi:[10.1002/etc.5620140813](https://doi.org/10.1002/etc.5620140813)
16. Nott MA, Driscoll HE, Takeda M, Vangala M, Corsi SR, Tighe SW. Advanced biofilm analysis in streams receiving organic deicer runoff. *PLoS ONE.* 2020;15:e0227567. doi:[10.1371/journal.pone.0227567](https://doi.org/10.1371/journal.pone.0227567)
17. Exton B, Hassard F, Medina-Vaya A, Grabowski RC. Undesirable river biofilms: The composition, environmental drivers, and occurrence of sewage fungus. *Ecol Indic.* 2024;161:111949. doi:[10.1016/j.ecolind.2024.111949](https://doi.org/10.1016/j.ecolind.2024.111949)
18. Corsi SR, Geis SW, Loyo-Rosales JE, Rice CP, Sheesley RJ, Failey GG, et al. Characterization of aircraft deicer and anti-icer components and toxicity in airport snowbanks and snow-melt runoff. *Environ Sci Technol.* 2006;40:3195–202. doi:[10.1021/es052028m](https://doi.org/10.1021/es052028m)
19. Barash S, Covington J, Tamulonis C. Preliminary data summary airport deicing operations (revised). Washington: United States Environmental Protection Agency; 2000. 447 p.
20. Johnson EP. Aircraft de-icer: Recycling can cut carbon emissions in half. *Environ Impact Assess Rev.* 2012;32:156–64. doi:[10.1016/j.eiar.2011.08.001](https://doi.org/10.1016/j.eiar.2011.08.001)
21. Bausmith DS, Neufeld RD. Soil biodegradation of propylene glycol based aircraft deicing fluids. *Water Environ Res.* 1999;71(4):459–64. doi:[10.2175/106143097X121997](https://doi.org/10.2175/106143097X121997)
22. Lucas R, Earl ER, Babatunde AO, Bockelmann-Evans BN. Constructed wetlands for stormwater management in the UK: A concise review. *Civ Eng Environ Syst.* 2015;32:251–68. doi:[10.1080/10286608.2014.958472](https://doi.org/10.1080/10286608.2014.958472)
23. Schoenberg T, Veltman S, Switzenbaum M. Kinetics of anaerobic degradation of glycol-based Type I aircraft deicing fluids. *Biodegradation.* 2001;12:59–67. doi:[10.1023/A:1011961214180](https://doi.org/10.1023/A:1011961214180)
24. Adeola S, Revitt M, Shutes B, Garelick H, Jones H, Jones C. Constructed wetland control of BOD levels in airport runoff. *Int J Phytoremed.* 2009;1:1–10. doi:[10.1080/15226510802363220](https://doi.org/10.1080/15226510802363220)
25. Aguinaco A, Pocostales JP, García-Araya JF, Beltrán FJ. Decomposition of hydrogen peroxide in the presence of activated carbons with different characteristics. *J Chem Technol Biotechnol.* 2011;86(4):595–600. doi:[10.1002/jctb.2560](https://doi.org/10.1002/jctb.2560)
26. Khalil LB, Girgis BS, Tawfik TAM. Decomposition of H<sub>2</sub>O<sub>2</sub> on activated carbon obtained from olive stones. *J Chem Technol Biotechnol.* 2001;76(11):1132–40. doi:[10.1002/jctb.481](https://doi.org/10.1002/jctb.481)
27. Armstrong DA, Huie RE, Koppenol WH, Lyman SV, Merényi G, Neta P, et al. Standard electrode potentials involving radicals in aqueous solution: Inorganic radicals (IUPAC Technical Report). *Pure Appl Chem.* 2015;87:1139–50. doi:[10.1515/pac-2014-0502](https://doi.org/10.1515/pac-2014-0502)
28. Kulišřáková A. Removal of pharmaceutical micropollutants from real wastewater matrices by means of photochemical advanced oxidation processes – A review. *J Water Process Eng.* 2023;53:103727. doi:[10.1016/j.jwpe.2023.103727](https://doi.org/10.1016/j.jwpe.2023.103727)
29. Liu P, Wu Z, Abramova AV, Cravotto G. Sonochemical processes for the degradation of antibiotics in aqueous solutions: A review. *Ultrason Sonochem.* 2021;74:105566. doi:[10.1016/j.ultsonch.2021.105566](https://doi.org/10.1016/j.ultsonch.2021.105566)
30. Wang Y, Liu M, Miao Q, Wu P, He J, Liu C, et al. Rapid green degradation of ethylene glycol-based antifreeze wastewater via a coupled photolytic and photocatalytic double-pathway mechanism. *J Water Process Eng.* 2025;71:107191. doi:[10.1016/j.jwpe.2025.107191](https://doi.org/10.1016/j.jwpe.2025.107191)
31. Yuan Q, Qu S, Li R, Huo ZY, Gao Y, Luo Y. Degradation of antibiotics by electrochemical advanced oxidation processes (EAOPs): Performance, mechanisms, and perspectives. *Sci Total Environ.* 2023;856:159092. doi:[10.1016/j.scitotenv.2022.159092](https://doi.org/10.1016/j.scitotenv.2022.159092)
32. Shokri A, Fard MS. A critical review in Fenton-like approach for the removal of pollutants in the aqueous environment. *Environ Chall.* 2022;7:100534. doi:[10.1016/j.envc.2022.100534](https://doi.org/10.1016/j.envc.2022.100534)
33. Fazliev T, Lyulyukin M, Kozlov D, Selishchev D. Kinetic aspects of ethylene glycol degradation using UV-C activated hydrogen peroxide (H<sub>2</sub>O<sub>2</sub>/UV-C). *Molecules.* 2025;30:49. doi:[10.3390/molecules30010049](https://doi.org/10.3390/molecules30010049)
34. Liu Z, Hosseinzadeh S, Wardenier N, Verheust Y, Chys M, Hulle SV. Combining ozone with UV and H<sub>2</sub>O<sub>2</sub> for the degradation of micropollutants from different origins: Lab-scale analysis and optimization. *Environ Technol.* 2019;40:3773–82. doi:[10.1080/09593330.2018.1491630](https://doi.org/10.1080/09593330.2018.1491630)
35. Ghaly MY, Härtel G, Mayer R, Haseneder R. Photochemical oxidation of p-chlorophenol by UV/H<sub>2</sub>O<sub>2</sub> and photo-Fenton process. A comparative study. *Waste Manag.* 2001;21:41–7. doi:[10.1016/S0956-053X\(00\)00070-2](https://doi.org/10.1016/S0956-053X(00)00070-2)
36. McGinnis DB, Adams DV, Middlebrooks JE. Degradation of Ethylene Glycol Using Fenton's Reagent and UV. *Chemosphere* 2001, 45, 101–108. doi:[10.1016/S0045-6535\(00\)00597-X](https://doi.org/10.1016/S0045-6535(00)00597-X).
37. Priyadarshini M, Ahmad A, Das I, Ghangrekar MM, Dutta BK. Efficacious degradation of ethylene glycol by ultraviolet activated persulphate: Reaction kinetics, transformation mechanisms, energy demand, and toxicity assessment. *Environ Sci Pollut Res.* 2023;30:85071–86. doi:[10.1007/s11356-023-27596-9](https://doi.org/10.1007/s11356-023-27596-9)
38. Wang J, Wang S. Effect of inorganic anions on the performance of advanced oxidation processes for degradation of organic contaminants. *Chem Eng J.* 2021;411:128392. doi:[10.1016/j.cej.2020.128392](https://doi.org/10.1016/j.cej.2020.128392)
39. Machado F, Teixeira ACSC, Ruotolo LAM. Critical review of Fenton and photo-Fenton wastewater treatment processes over the last two decades. *Int J Environ Sci Technol.* 2023;20:13995–4032. doi:[10.1007/s13762-023-05015-3](https://doi.org/10.1007/s13762-023-05015-3)
40. Lee C, Seo J, Pham AL-T. The Photo-Fenton System. In *Springer Handbook of Inorganic Photochemistry*; Bahnmann, D., Patrocínio, A.O.T., Eds.; Springer International Publishing: Cham, 2022. pp. 1719–1734
41. Tokumura M, Morito R, Hatayama R, Kawase Y. Iron redox cycling in hydroxyl radical generation during the photo-Fenton oxidative degradation: Dynamic change of hydroxyl radical concentration. *Appl Catal B Environ.* 2011;106:565–76. doi:[10.1016/j.apcatb.2011.06.017](https://doi.org/10.1016/j.apcatb.2011.06.017)
42. Carra I, García Sánchez JL, Casas López JL, Malato S, Sánchez Pérez JA. Phenomenological study and application of the

- combined influence of iron concentration and irradiance on the photo-Fenton process to remove micropollutants. *Sci Total Environ.* 2014;478:123–32. doi:[10.1016/j.scitotenv.2014.01.066](https://doi.org/10.1016/j.scitotenv.2014.01.066)
43. Hermosilla D, Cortijo M, Huang CP. Optimizing the treatment of landfill leachate by conventional Fenton and photo-Fenton processes. *Sci Total Environ.* 2009;407:3473–81. doi:[10.1016/j.scitotenv.2009.02.009](https://doi.org/10.1016/j.scitotenv.2009.02.009)
44. Khatri N, Tyagi S, Rawtani D. Recent strategies for the removal of iron from water: A review. *J Water Process Eng.* 2017;19:291–304. doi:[10.1016/j.jwpe.2017.08.015](https://doi.org/10.1016/j.jwpe.2017.08.015)
45. Fakhfekh R, Chabanon E, Mangin D, Amar RB, Charcosset C. Removal of iron using an oxidation and ceramic microfiltration hybrid process for drinking water treatment. *Desalin Water Treat.* 2017;66:210–20. doi:[10.5004/dwt.2017.20225](https://doi.org/10.5004/dwt.2017.20225)
46. Modin H, Persson KM, Andersson A, van Praagh M. Removal of metals from landfill leachate by sorption to activated carbon, bone meal and iron fines. *J Hazard Mater.* 2011;189:749–54. doi:[10.1016/j.jhazmat.2011.03.001](https://doi.org/10.1016/j.jhazmat.2011.03.001)
47. Chaturvedi S, Dave PN. Removal of iron for safe drinking water. *Desalination.* 2012;303:1–11. doi:[10.1016/j.desal.2012.07.003](https://doi.org/10.1016/j.desal.2012.07.003)
48. Sui X, Zhou Y, Zhang F, Chen J, Zhu Z, Yu XY. Deciphering the aqueous chemistry of glyoxal oxidation with hydrogen peroxide using molecular imaging. *Phys Chem Chem Phys.* 2017;19:20357–66. doi:[10.1039/C7CP02071F](https://doi.org/10.1039/C7CP02071F)
49. Sui X, Xu B, Yu J, Kostko O, Ahmed M, Yu XY. Studying interfacial dark reactions of glyoxal and hydrogen peroxide using vacuum ultraviolet single photon ionization mass spectrometry. *Atmosphere.* 2021;12:338. doi:[10.3390/atmos12030338](https://doi.org/10.3390/atmos12030338)
50. Eugene AJ, Xia SS, Guzman MI. Aqueous photochemistry of glyoxylic acid. *J Phys Chem A.* 2016;120:3817–26. doi:[10.1021/acs.jpca.6b00225](https://doi.org/10.1021/acs.jpca.6b00225)
51. Zhang F, Yu X, Chen J, Zhu Z, Yu XY. Dark air–liquid interfacial chemistry of glyoxal and hydrogen peroxide. *Clim Atmos Sci.* 2019;2:28. doi:[10.1038/s41612-019-0085-5](https://doi.org/10.1038/s41612-019-0085-5)
52. Santoss L, Lima Poli A, Schmitt Cavalheiro C, Neumann M. The UV/H<sub>2</sub>O<sub>2</sub> - photodegradation of poly(ethyleneglycol) and model compounds. *J Braz Chem Soc.* 2009;20(8):14647–72. doi:[10.1590/S0103-50532009000800012](https://doi.org/10.1590/S0103-50532009000800012)
53. Fazliev TR, Bukhtiyarov AV, Selishchev DS. Photocatalytic formation of hydrogen peroxide in aqueous suspensions of titanium dioxide supported with palladium. *Kinet Catal.* 2024;65:672–81. doi:[10.1134/S0023158424602432](https://doi.org/10.1134/S0023158424602432)
54. Payne JH, Lemon GF Jr. The oxidation of aldehydes with hydrogen peroxide. *J Am Chem Soc.* 1941;63:226–8. doi:[10.1021/ja01846a053](https://doi.org/10.1021/ja01846a053)
55. Magneron I, Mellouki A, Le Bras G, Moortgat GK, Horowitz A, Wirtz K. Photolysis and OH-initiated oxidation of glycolaldehyde under atmospheric conditions. *J Phys Chem A.* 2005;109:4552–61. doi:[10.1021/jp044346y](https://doi.org/10.1021/jp044346y)
56. Zuo Y, Hoigne J. Photochemical decomposition of oxalic, glyoxylic and pyruvic acid catalysed by iron in atmospheric waters. *Atmos Environ.* 1994;28:1231–9. doi:[10.1016/1352-2310\(94\)90270-4](https://doi.org/10.1016/1352-2310(94)90270-4)
57. Santambrogio M, Perrucci G, Trueba M, Trasatti SP, Casaletto MP. Effect of major degradation products of ethylene glycol aqueous solutions on steel corrosion. *Electrochim Acta.* 2016;203:439–50. doi:[10.1016/j.electacta.2016.03.144](https://doi.org/10.1016/j.electacta.2016.03.144)
58. Jeong J, Yoon J. pH effect on OH radical production in photo/ferrioxalate system. *Water Res.* 2005;39:2893–900. doi:[10.1016/j.watres.2005.05.014](https://doi.org/10.1016/j.watres.2005.05.014)
59. Aristova NA, Karpel Vel Leitner N, Piskarev IM. Degradation of formic acid in different oxidative processes. *High Energy Chem.* 2002;36:197–202. doi:[10.1023/A:1015385103605](https://doi.org/10.1023/A:1015385103605)
60. Vel Leitner NK, Dore M. Hydroxyl radical induced decomposition of aliphatic acids in oxygenated and deoxygenated aqueous solutions. *J Photochem Photobiol A.* 1996;99:137–43. doi:[10.1016/S1010-6030\(96\)04360-2](https://doi.org/10.1016/S1010-6030(96)04360-2)
61. Ahile UJ, Wuana RA, Itodo AU, Sha’Ato R, Dantas RF. Stability of iron chelates during photo-Fenton process: The role of pH, hydroxyl radical attack and temperature. *J Water Process Eng.* 2020;36:101320. doi:[10.1016/j.jwpe.2020.101320](https://doi.org/10.1016/j.jwpe.2020.101320)
62. Vallés I, Santos-Juanes L, Amat AM, Moreno-Andrés J, Arques A. Effect of salinity on UVA-Vis light driven photo-Fenton process at acidic and circumneutral pH. *Water.* 2021;13:1315. doi:[10.3390/w13091315](https://doi.org/10.3390/w13091315)
63. Rozas O, Contreras D, Mondaca MA, Pérez-Moya M, Mansilla HD. Experimental design of Fenton and photo-Fenton reactions for the treatment of ampicillin solutions. *J Hazard Mater.* 2010;177:1025–30. doi:[10.1016/j.jhazmat.2010.01.023](https://doi.org/10.1016/j.jhazmat.2010.01.023)
64. Duesterberg CK, Mylon SE, Waite TD. pH effects on iron-catalyzed oxidation using Fenton’s reagent. *Environ Sci Technol.* 2008;42:8522–7. doi:[10.1021/es801720d](https://doi.org/10.1021/es801720d)
65. Puzyn T, Mostrag A. Organic Pollutants Ten Years After the Stockholm Convention: Environmental and Analytical Update. InTech: Rijeka; 2012. 472 p.
66. Laurence GS, Thornton AT. Kinetics of oxidation of transition-metal ions by halogen radical anions. Part III. The oxidation of manganese(II) by dibromide and dichloride ions generated by flash photolysis. *J Chem Soc Dalton Trans.* 1973:1637–44. doi:[10.1039/DT9730001637](https://doi.org/10.1039/DT9730001637)